Flight testing of incremental backstepping based control laws with angular accelerometer feedback

Keijzer, Twan; Looye, Gertjan; Chu, Qiping; van Kampen, Erik-jan

Important note
To cite this publication, please use the final published version (if applicable).
Please check the document version above.

Flight Testing of Incremental Backstepping based Control Laws with Angular Accelerometer Feedback

Twan Keijzer*†, Gertjan Looye‡, Qiping Chu§ and Erik-Jan van Kampen¶

DLR, German Aerospace Center, 82234 Wessling, Germany

Delft University of Technology, P.O. Box 5058, 2626HS Delft, The Netherlands

This paper discusses the design, implementation and flight testing of an incremental Backstepping (IBS) based manual flight control law with angular accelerometer (AA) feedback. The main advantages of incremental control laws is that they only require a partial model of the system and are of low complexity. Incremental control laws for aircraft rotational motion, however, need angular acceleration measurements to compute the control increments. Previously, estimates based on angular rate measurements were used for this. The newly implemented AA feedback is expected to improve the performance by decreasing the sensor delay. The manual control laws command roll rate/angle, side slip angle and angle of attack and have been implemented on a Cessna Citation II aircraft, which is equipped with an experimental fly-by-wire system. The IBS based control law has an integrated integral control term and uses Pseudo Control Hedging to handle actuator saturations. A load factor outerloop has been added to improve the manual flyability. The IBS based control law has highly satisfactory performance in flight. Test manoeuvres included standard roll and load factor commands and asymmetric thrust handling. Fault tolerance has been compared in a nonlinear simulation for the controllers with and without AA feedback in simulation. In general, the angular accelerometer feedback improved the tolerance to mismatch substantially.

Nomenclature

A_x, A_y, A_z	Linear accelerations along body x,y, and z axis, g
$C_{D,Y,L}$	Dimensionless Force coefficients along stability x,y, and z axis
$C_{l,m,n}$	Dimensionless Moment coefficients around body x,y, and z axis
$\boldsymbol{F}_A, \boldsymbol{F}_T$	Aerodynamic and Propulsive Force vectors, N
G	Control dependent part of the model
$\boldsymbol{I}$	Inertia matrix, kgm^2
K	Gain
$\boldsymbol{M}_A, \boldsymbol{M}_T$	Aerodynamic and Propulsive Moment vectors, Nm
M	Mach number
S	Wing surface area, m^2
$\mathbb{T}_{AB}$	Rotation Matrix from reference frame B to A
$\boldsymbol{V}$	Velocity vector, m/s
$V_{\text{TAS}}, V_{\text{CAS}}$	True air speed and calibrated air speed, m/s
V	Lyapunov function
W	Weight, N
X, Y, Z	Position, m
b	Wing span, m^2
$\bar{c}$	Mean aerodynamic chord, m
$\boldsymbol{f}$	Control independent part of the model
f_x, f_y, f_z	Specific forces along body x,y, and z axis, g
g	Gravitational acceleration, m/s^2

*Graduate Student, Faculty of Aerospace Engineering, Control and Simulation Division, Delft University of Technology

†Intern, Department of Aircraft System Dynamics, Institute of System Dynamics and Control, German Aerospace Center

‡Head, Department of Aircraft System Dynamics, Institute of System Dynamics and Control, German Aerospace Center

§Associate Professor, Faculty of Aerospace Engineering, Control and Simulation Division, Delft University of Technology

¶Assistant Professor, Faculty of Aerospace Engineering, Control and Simulation Division, Delft University of Technology

h	Height, m
m	Mass, kg
n_z	Load factor in body z direction, g
$\boldsymbol{p}$	Parameter uncertainty vector
p, q, r	Roll, pitch and yaw rate around the body x,y, and z axis, rad/s
$\boldsymbol{u}$	Control input vector
u, v, w	Velocity components along body x,y, and z axis, m/s
$\boldsymbol{u}_d$	Desired control input vector
$\boldsymbol{x}, \boldsymbol{x}_c$	State vector and control variables
$\boldsymbol{y}_c$	Output vector
z	Tracking error
α, β, γ	Angle of attack, sideslip angle and flight path angle, rad
$\delta_a, \delta_e, \delta_r$	Aileron, Elevator, and Rudder deflection, rad
Δ	Increment
ζ	Damping ratio
ϕ, θ, ψ	Euler Roll, pitch, and yaw angle, rad
λ	Time delay, s
ν	Virtual control input vector
ν_h	Hedging term
ρ	Air density, kg/m^3
τ	Time constant, delay, s
ω	Angular rate vector, rad/s
ξ	Command filtered error introduced by the command filter
Superscript	
b	Body
s	Stability

I. Introduction

Commercial aviation flight control systems are designed to support pilots with augmented stability and control. Classical control techniques have difficulties to continue providing support in case of changes in aircraft behaviour due to e.g. component failures or weather conditions, like icing. In these cases classical control systems revert to revisionary control modes or even to direct control. This causes the pilot workload to be increased, not only due to the failure, but also due to the change in aircraft control. Research currently focusses on maintaining functionality when faults occur and the flight control system support is needed most.

Nonlinear control methods, such as Nonlinear Dynamic Inversion (NDI) and Backstepping (BKS), aim to globally linearise the system dynamics by inversion of the aircraft model. This eliminates the need for gain-scheduling, forming a uniform control law over the full flight envelope. These methods are however highly model dependent and, therefore, need on-line model identification to qualify as fault tolerant. This identification adds a lot of complexity to the control law, and makes them difficult to certify.

Fig. 1   PH-LAB Cessna Citation II

As an alternative, Incremental Nonlinear Dynamic Inversion (INDI) and Incremental Backstepping (IBS) aim to improve the fault tolerance by reducing the model dependency. These control laws use synchronous estimates of the control deflections and angular accelerations, to rewrite the model in an incremental form, which is only dependent on the control effectiveness matrix. For the implementation of these methods, a high update frequency and precise synchronisation are required. For this reason, the feasibility of implementing incremental control laws on conventional Flight Control Computers seemed doubtful at first. It has, however, been proven to work in previous flight tests. [1–3]

Even though the core of both IBS and INDI based control laws is a partial model inversion, they differ significantly in theoretical basis and capabilities. INDI is mainly suited for control of variables with a relative degree of one with

2

respect to the input. Unlike INDI, IBS allows for integrated, multi-loop controller design. It is therefore better suited for control of variables with a relative degree higher than one, such as aerodynamic angles or load factors. Furthermore, as IBS based control design is derived from Lyapunov stability functions, the stability of the resulting control law is guaranteed.

Previous Flight Tests
Both INDI and IBS based control laws have been flight tested successfully on different platforms. INDI was first flight tested on the FASER UAV by the German Aerospace Centre (DLR), in cooperation with Delft University of Technology. [1] Others have performed further flight tests [4, 5], and most recently Grondman has implemented INDI on the CS-25 certified PH-LAB Cessna Citation II. [3] IBS has yet only been flight tested by Van Ekeren on the FASER UAV. [2]

Recently Delft University of Technology has acquired SR-207RFR angular accelerometers, aiming to implement them on the PH-LAB Cessna Citation II. A model was made by Jatiningrum using frequency-Response Measurements of the angular accelerometers on a test bench. [6] Using the direct angular acceleration measurements provided by these sensors, instead of those derived from the angular rate measurements, is expected to improve the performance of both INDI and IBS by reducing the system delay. [7]

Contribution
The contribution of this paper is twofold. Firstly, the design, implementation, and flight test results of an IBS based controller for the PH-LAB Cessna Citation II (see figure 1) are presented. The design is made with the objective to demonstrate the practical use and advantages of IBS based control in flight on a CS-25 certified aircraft.

Secondly, the implementation of angular accelerometers and their benefits for INDI and IBS based control are presented in this paper. The angular acceleration estimates, which these models need are then no longer based on angular rate measurements. Instead they are replaced by angular accelerometer measurements. In order to make comparison possible, the angular accelerometers are implemented with the least amount of change to the controllers.

Outline
This paper is structured as follows. First, the objectives of the research and the design choices made are presented in section II. Subsequently, the aircraft model is presented in section III. In section IV the derivation and assumptions for INDI and IBS are shown. In section V the other controller subsystems are discussed and final controller design is presented. Furthermore, this section contains the results regarding the tolerance of the controllers against model mismatch. In section VI, the experimental setup is outlined, followed by the flight test results in section VII. The paper is concluded in section VIII.

II. Objectives and Design

The chosen platform and contribution, as stated in section I, lead to some design choices that affect the structure of the designed controllers. Some of these design choices affect the inherent structure of the controller as described in section IV. Other design choices are implemented as additional modules which are described in section V.

The first objective of this research is to demonstrate the practical use and advantages of IBS based control in flight on a CS-25 certified aircraft. This requires an IBS based manual control law with the following properties. First, to demonstrate the advantages of IBS based control it should make use of the integrated multi-loop control design, for which IBS allows. Therefore, the control variables should be of a relative degree of at least two with respect to the output and should have relatively complex dynamics for each relative degree. Secondly, the innermost loop of the IBS controler should control angular rates. This creates the need for angular acceleration measurements, which is what drives the angular accelerometer implementation in the second objective. Thirdly, the controller should be able to handle actuator saturation, without knowing the deflection at which saturation occurs. In the PH-LAB fly-by-wire system the allowable actuator deflections are small and limited by the torque on the actuator servo. This means that saturation occurs regularly and at a different deflection for different flight conditions. As fourth requirement, the handling qualities of the controller should be sufficient for the pilots to perform the required manoeuvres. Last, the controller should be stable and tolerant to model mismatch.

The second objective is to assess the benefit of angular accelerometer feedback for incremental controllers, represented in this research by INDI and IBS. This is done by replacing the currently used angular acceleration estimates based on angular rate measurements with angular accelerometer feedback. The implementation is, therefore, required to

have the following properties. Firstly, the angular accelerometer feedback should be used in both the INDI and IBS controller. Secondly, to ensure a fair comparison, the controllers with and without angular accelerometer measurements should be sufficiently similar. Lastly, signal noise and structural vibrations should be handled with minimal impact on the controller performance.

Based on the requirements, for this research, the following controllers are needed. An INDI based controller and an IBS based controller, both working with and without angular accelerometer feedback. The INDI based controller without angular accelerometers is taken to be the one designed and tested by Grondman [3]. This controller is taken as the state of the art and has not been changed in order to ensure a working baseline controller.

This baseline controller uses INDI with a two degree of freedom outer loop design. In pitch and roll, the pilot has rate command attitude hold (RCAH) control at lower angles and direct attitude control at higher angles. RCAH entails that the pilot commands angular rates and the controller ensures that the attitude tracks the integrated rate command. Thus, if no command is given the attitude is held even in case of disturbances. In yaw, the controller stabilises the sideslip angle around zero. Furthermore, the control law uses Pseudo Control Hedging (PCH) to handle actuator saturation. The outer loop gains are tuned using the Multi Objective Parameter Synthesis tool (MOPS). [8]

The angular accelerometers are implemented in the INDI and IBS controllers with the least possible change. Only the synchronisation modules have to be changed to adapt to the new sensor and filtering delays. In this way it can be ensured that a fair comparison can be made between the controllers. Furthermore a module for the angular accelerometer measurements has to be added to the signal filtering to handle noise and structural vibrations. The filter is chosen such that the noise level of the filtered measured angular accelerations is close to that of the filtered estimated angular accelerations.

For the IBS based controller, first, the control variables have to be decided upon. The control variables should be chosen with a relative degree of at least two and a relatively complex relation for each relative degree. Furthermore, control variables should be chosen which have a relation with the angular rates. As explained before, this introduces the need for angular accelerometer feedback. There are multiple possibilities for control variables that match this description, but in this research the control variables chosen for the integrated IBS control law are $[\phi \ \alpha \ \beta]^T$.

To improve the handling quality of the controller, the IBS control law is extended with a stand-alone outer loop. The handling quality when controlling angle of attack is poor, because the needed angle of attack changes with flight condition. Therefore, in pitch direction a load factor controller has been made using an approximate relation between angle of attack and load factor to estimate a command and an integral controller to solve any discrepancies. Furthermore, in roll direction, the outer-loop allows the pilot to have the same combination of RCAH and direct attitude control functionality as for the INDI based controller. In yaw, the control law stabilises sideslip, without changes to the command needed in the outer loop.

As is done for the INDI controller, the required handling of control saturation is achieved by means of Pseudo Control Hedging (PCH). PCH was introduced by Johnson et al. [9] and was first applied to INDI by Grondman [3]. PCH is chosen for this application, because the deflection at which saturation occurs does not need to be known when using PCH. To the authors knowledge PCH is the only method with this property.

Lastly, the IBS based controller design is required to be stable and robust against model mismatch. This becomes increasingly difficult for larger platforms, as they have more system delays, which reduces the applicability of the assumptions. The IBS controller can be adapted in two ways to still ensure stable and robust behaviour. Firstly, the Control Lyapunov Function (CLF), on which the control law is based, can be extended to include additional control terms. The simplest CLF ,with only a proportional control term, which has been used, for example, by van Ekeren in his implementation on the Phasor UAV [2], does not suffice for the larger Cessna Citation II. For this aircraft, additional control needs to be integrated in the IBS controller. In order to do this the Lyapunov function is extended to include an integral control term in the IBS control law. This has been done before in simulation on a nonlinear missile model by Sonneveld. [10]. Secondly, the gains in the controller can be tuned. Due to time constraints, the gains for the IBS controller are tuned manually, but care has been taken to stay well away of possible oscillations and instabilities. If the time would have allowed, a more automatic and structured tuning method, like MOPS [8] would be preferable.

III. Aircraft Model

The aircraft chosen for this research is the PH-LAB Cessna Citation II, jointly operated by Delft University of Technology and the Netherlands Aerospace Centre (NLR). The aircraft was originally designed as an 8-passenger business jet, but is extensively modified to serve as a multi-purpose airborne research platform. A picture of the PH-LAB can be found in figure 1. In this section first the DASMAT based aircraft model is discussed, followed by the sensor, actuator and mass

models, which were added later.

A. Equations of Motion

The aircraft equations of motion are implemented for the Cessna Citation 500 in a model developed using the Delft University Aircraft Simulation Model and Analysis Tool (DASMAT) in MATLAB/Simulink. [11] This model has a 7-13% Relative Root Mean Square Error from a validation dataset for the non-dimensional force and moment coefficients of the Cessna Citation II. [12] The geometric parameters of the model have been adapted to be able to apply these coefficients to the Cessna Citation II.

In the DASMAT model, the motion of the aircraft is described by the combined translational and rotational dynamics equations of motion as presented in equations 1 and 2. In these equations, the vectors are expressed in the right-handed downward-forward-starboard aircraft body reference frame. The velocity and angular rate vectors are defined as $V = [u \ v \ w]^T$ and $\omega = [p \ q \ r]^T$ respectively. The vector g is the gravitational acceleration vector rotated to body frame as defined in equation 3 using the pitch and roll angles θ and ϕ.

$$\dot{V} = \frac{1}{m}[F_A(x, u, p) + F_T(x, u_T, p)] - \omega \times V + g \tag{1}$$

$$\dot{\omega} = I(p)^{-1}[M_A(x, u, p) + M_T(x, u_T, p) - \omega \times I(p)\omega] \tag{2}$$

$$g = \mathbb{T}_{bE} \begin{bmatrix} 0 \\ 0 \\ g \end{bmatrix} = \begin{bmatrix} -\sin(\theta) \\ \cos(\theta)\sin(\phi) \\ \cos(\theta)\cos(\phi) \end{bmatrix} g \tag{3}$$

The rest of the variables in the equations of motion are model dependent, and thus depend on parameter vector p. Matrix I is shown in equation 4 and contains the moments of inertia, which are simplified assuming symmetry in the xy-plane. The force and moment terms are divided in an aerodynamic $(_A)$ and a propulsion related $(_T)$ term. These forces and moments depend, in addition to the model parameters p, on the aircraft state x, and the control input u (of which u_T is a subset related to propulsion). In the control law development, the propulsion control input is considered as an aircraft state as it is manually controlled and in nominal flight only changing slowly.

$$I(p) = \begin{bmatrix} \bar{I}_{xx} & 0 & -\bar{I}_{xz} \\ 0 & \bar{I}_{yy} & 0 \\ -\bar{I}_{xz} & 0 & \bar{I}_{zz} \end{bmatrix} \tag{4}$$

The aerodynamic forces and moments are defined from the non-dimensional force and moment coefficients in stability frame as in equations 5 and 6. These are rotated and translated to the body frame as shown in equation 7 and 8. The non-dimensional coefficients in these equations are taken from lookup tables, which depend on the aircraft state.

$$F_A^s = \frac{1}{2}\rho V_{TAS}^2 S \begin{bmatrix} -C_D \\ C_Y \\ -C_L \end{bmatrix} \tag{5} \qquad M_A^s = \frac{1}{2}\rho V_{TAS}^2 S \begin{bmatrix} bC_l \\ cC_m \\ bC_n \end{bmatrix} \tag{6}$$

$$F_A^b = \mathbb{T}_{bs} F_A^s \tag{7} \qquad M_A^b = \mathbb{T}_{bs} M_A^s + \Delta l_{cg} \times \mathbb{T}_{bs} F_A^s \tag{8}$$

The rotational kinematics equation describes the attitude of the aircraft in the earth fixed reference frame. This equation only entails a simple rotations and is shown in equation 9.

$$\begin{bmatrix} \dot{\phi} \\ \dot{\theta} \\ \dot{\psi} \end{bmatrix} = \mathbb{C}_{Eb}\omega \quad , \text{where} \quad \mathbb{C}_{Eb} = \begin{bmatrix} 1 & \sin(\phi)\tan(\theta) & \cos(\phi)\tan(\theta) \\ 0 & \cos(\phi) & -\sin(\phi) \\ 0 & \sin(\phi)\sec(\theta) & \cos(\phi)\sec(\theta) \end{bmatrix} \tag{9}$$

For the derivation of the IBS control law it is useful to have equations for the dynamics of the control variables $[\phi \ \alpha \ \beta]^T$ directly. These can be derived from the equalities in equation 10 and their time derivatives as shown in equation 11. Substituting all body velocities and their derivatives from equations 10 and 1 in equation 11 gives, when simplified, the relations in equation 12.

$$V = |\boldsymbol{V}| = \sqrt{u^2 + v^2 + w^2} \qquad u = V \cos \alpha \cos \beta$$
$$\alpha = \arctan \frac{w}{u} \qquad \Leftrightarrow \qquad v = V \sin \beta \qquad (10)$$
$$\beta = \arcsin \frac{u}{V} \qquad w = V \sin \alpha \cos \beta$$

$$\dot{V} = \frac{1}{V}(u\dot{u} + v\dot{v} + w\dot{w})$$
$$\dot{\alpha} = \frac{1}{u^2 + w^2}(u\dot{w} - w\dot{u}) \qquad (11)$$
$$\dot{\beta} = \frac{1}{V^2 \cos \beta}(\dot{v}V - v\dot{V})$$

$$\dot{\alpha} = q - p \cos \alpha \tan \beta - r \sin \alpha \tan \beta + \frac{1}{V \cos \beta}\left[A_x \sin \alpha + A_z \cos \alpha + g_3\right]g$$
$$\dot{\beta} = p \sin \alpha - r \cos \alpha + \frac{1}{V}\left[A_x \cos \alpha \sin \beta + A_y \cos \beta - A_z \sin \alpha \sin \beta + g_2\right]g \qquad (12)$$

Here the relation for $\dot{V}$ is not shown as it is not needed. $A_\bullet$ in equation 12 are the linear accelerometer measurements along each body axis including the normalised thrust $\boldsymbol{F}_T$. g_2 and g_3 are defined in equation 13.

$$g_2 = \cos \alpha \sin \beta \sin \theta + \cos \beta \sin \phi \cos \theta - \sin \alpha \sin \beta \cos \phi \cos \theta$$
$$g_3 = \sin \alpha \sin \theta + \cos \alpha \cos \phi \cos \theta \qquad (13)$$

B. Sensor Models

Most sensors of the PH-LAB have been modelled by Grondman and Van 't Veld [3, 13] by adding a noise and bias to a delayed signal. This signal is discretised using the sensor's resolution and is fed back into the controller at a certain sampling frequency. The parameter values used for these models are shown in table 1.

Table 1 Sensor characteristics PH-LAB [3]

Signal	Noise (σ^2)	Bias	Resolution	Delay [ms]	Sampling rate [Hz]
$p, q, r, \dot{\theta}, \dot{\phi}, \dot{\psi}$ [rad/s]	$4.0 \cdot 10^{-7}$	$3.0 \cdot 10^{-5}$	$6.8 \cdot 10^{-7}$	90	52
θ, ϕ [rad]	$1.0 \cdot 10^{-9}$	$4.0 \cdot 10^{-3}$	$9.6 \cdot 10^{-7}$	90	52
A_x, A_y, A_z [g]	$1.5 \cdot 10^{-5}$	$2.5 \cdot 10^{-3}$	$1.2 \cdot 10^{-4}$	117	52
$V_{\text{TAS}}, V_{\text{CAS}}$ [m/s]	$8.5 \cdot 10^{-4}$	2.5	$3.2 \cdot 10^{-2}$	300	16, 8
h [m]	$4.5 \cdot 10^{-3}$	$8.0 \cdot 10^{-3}$	$3.0 \cdot 10^{-1}$	300	16
$\dot{h}$ [m/s]	$5.5 \cdot 10^{-4}$	$4.5 \cdot 10^{-2}$	$8.1 \cdot 10^{-2}$	300	16
M [-]	$1.0 \cdot 10^{-8}$	$7.0 \cdot 10^{-7}$	$6.3 \cdot 10^{-5}$	300	8
$\delta_a, \delta_e, \delta_r$ [rad]	$5.5 \cdot 10^{-7}$	$2.4 \cdot 10^{-3}$	-	~0	100
$\alpha_{boom}, \beta_{boom}$ [rad]	$7.5 \cdot 10^{-8}$	$1.8 \cdot 10^{-3}$	$9.6 \cdot 10^{-5}$	100	100
α_{body} [rad]	$4.0 \cdot 10^{-10}$	-	$1.0 \cdot 10^{-5}$	280	1000

The angular accelerometers installed in the experimental sensor bay of the PH-LAB especially for this research are of the type SR-207RFR and were modelled by Jatiningrum et al. [6]. In this research their 5th order non-minimum phase model is used.The transfer function of this model is shown in equation 14. This model is made using Frequency-Response Measurements of the angular accelerometers on a test bench. Based on this model a static delay of $15ms$ has been estimated to most accurately represent the delay introduced by the transfer function. This delay is used for synchronisation as discussed in section V.A.

$$\frac{\dot{\omega}_{\text{meas}}}{\dot{\omega}_{\text{act}}} = \frac{3983241.0s + 100970.7}{s^5 + 400.1s^4 + 104313.7s^3 + 14989513.1s^2 + 994565928.9s + 13463947.7} \qquad (14)$$

The static noise level of the angular accelerometers is determined to be $1.4703 \cdot 10^{-6}$ [rad/s^2] by Çakiroğlu [7] based on data from the research by Jatiningrum [6]. Furthermore the range, resolution and bias used are 10[rad/s^2], 0.001[rad/s^2] and ±0.01VDC $\mapsto$ 0.04rad/s^2 respectively. These values are taken from the sensor specifications as provided by Columbia Research Laboratories Inc.*

---

*https://www.crlsensors.com/product.cfm?cat=force-balance&sub=angular-accelerometers&prod=sr-207rfr

C. Actuator Model

In the aircraft model, two actuator models are included. A low-fidelity first order model and a high-fidelity model, which models individual components of the servo-actuator system.

Grondman has replaced the Citation 500 first order actuator model which was originally implemented in the DASMAT model [11] with a new first order actuator model based on flight test data from the PH-LAB Cessna Citation II. The model includes the physical actuator deflection and rate limits, and a transport delay (λ_{act}). The model is shown in equation 15.

$$\dot{\boldsymbol{\delta}}(t) = \text{sat}_{\dot{\delta}}\{\boldsymbol{\omega}_{\text{act}} \cdot \boldsymbol{u}(t - \lambda_{\text{act}}) - \boldsymbol{\omega}_{\text{act}}\text{sat}_{\delta}[\boldsymbol{\delta}(t)]\} \tag{15}$$

The high fidelity model is identified by Mulder et al. [14] and implemented in the DASMAT model by Pollack et al. [15]. This model very accurately describes the dynamics of the fly-by-wire system for the elevator and aileron channels. However, because the flight control system contains stiff dynamics, higher-order solvers and high computation rates are required to simulate the high fidelity model. Note that no high fidelity model for the rudder was identified.

The high fidelity model is based on a test campaign, including ground and flight tests, for identification of the individual control channels and autopilot servo system. The resulting model is largely linear, but does account for nonlinear behaviour such as Coulomb friction, nonlinear hinge moment aerodynamics and the torque based saturation for experimental control input.

D. Mass Model

An accurate on-line mass model of the Cessna Citation II has been identified by De Visser at al.[16]. Grondman et al. adapted this model for use in the modified DASMAT model. [3] The model provides aircraft inertia, mass and centre of gravity position taking into account passengers, payload and fuel. The model is updated using feedback of the used fuel and the fuel tank geometry.

IV. Incremental Nonlinear Control Laws

In this section the theoretical concepts behind the used control laws are reviewed. Where needed the chosen control variables and simplifying assumptions will be used in the derivation of the control laws to avoid unnecessary repetition. First Nonlinear Dynamic Inversion (NDI) and Incremental Nonlinear Dynamic Inversion (INDI) will be discussed followed by Backstepping (BKS) and Incremental Backstepping (IBS). At the end of the section Command Filtered Incremental Backstepping (CFIBS) will be introduced as an extension to IBS, which allows for practical implementation on complex systems.

A. Nonlinear Dynamic Inversion

The concept for NDI is to invert the input-output relation, such that the input can directly be derived from the reference output. In order to make this possible it is assumed that the aircraft model can be written in the control-affine form shown in equation 16. Furthermore, it is assumed that the output is equal to the state.

$$\dot{\boldsymbol{y}}_c = \dot{\boldsymbol{x}}_c = \boldsymbol{f}(\boldsymbol{x}, \boldsymbol{p}) + G(\boldsymbol{x}, \boldsymbol{p})\boldsymbol{u} \tag{16}$$

here $\boldsymbol{x}_c \in \mathbb{R}^m$ is the vector of control variables, which is a subgroup of the full state $\boldsymbol{x} \in \mathbb{R}^n$, $\boldsymbol{u} \in \mathbb{R}^m$ is the control input vector and $\boldsymbol{y}_c \in \mathbb{R}^m$ the part of the system output vector related to the control variables. Note that here we assumed that $\boldsymbol{u}$, $\boldsymbol{x}_c$, and $\boldsymbol{y}_c$ are equal in dimension, which is true for the current application, but not in general. $\boldsymbol{f}$ and $\boldsymbol{h}$ are functions with at least first order continuity describing the system and output dynamics respectively. G is the control effectiveness matrix and $\boldsymbol{p}$ is the vector of uncertain system parameters.

Now define $\boldsymbol{v}$ as the reference for $\dot{\boldsymbol{x}}_c$, and $\hat{\boldsymbol{x}}$ and $\hat{\boldsymbol{p}}$ as the state and parameter vectors as known by the controller. The NDI control law as shown in equation 17 is now found by inverting the state equation from equation 16. Here $\boldsymbol{u}_d$ is the desired control input, which is for the rest of the derivation assumed to be equal to the actual control input.

$$\boldsymbol{u}_d = G(\hat{\boldsymbol{x}}, \hat{\boldsymbol{p}})^{-1}[\boldsymbol{v} - \boldsymbol{f}(\hat{\boldsymbol{x}}, \hat{\boldsymbol{p}})] \tag{17}$$

If one substitutes the control law (Eq. 17) into equation 16, the resulting dynamics of the controlled system appear as in equation 18. It can be seen that if $\boldsymbol{x}$ and $\boldsymbol{p}$ are exactly known, the system dynamics are cancelled completely and $\dot{\boldsymbol{x}}_c = \boldsymbol{v}$. If the estimates $\hat{\boldsymbol{x}}$ and $\hat{\boldsymbol{p}}$ are off some non-linearities will remain in the closed loop behaviour.

$$\dot{x}_c = f(x, p) + G(x, p)G(\hat{x}, \hat{p})^{-1}[v - f(\hat{x}, \hat{p})] \tag{18}$$

B. Incremental Nonlinear Dynamic Inversion

In the step from NDI to Incremental Nonlinear Dynamic Inversion (INDI), the theoretical concept of inverting the input-output relation is not lost. However the model (Eq. 16) is replaced by its first order Taylor expansion, making it incremental. This is done in equation 19, where the variables with subscript $_0$ are of one timestep before the current.

$$\dot{x}_c \approx \dot{x}_{c,0} + \frac{\partial}{\partial x_c}[f(x, p) + G(x, p)u]\bigg|_{\substack{x=x_0 \\ u=u_0}} \underbrace{(x_c - x_{c,0})}_{\Delta x_c} + \frac{\partial}{\partial u}[f(x, p) + G(x, p)u]\bigg|_{\substack{x_c=x_{c,0} \\ u=u_0}} \underbrace{(u - u_0)}_{\Delta u} \tag{19}$$

For sufficiently small time steps it can now be assumed that the principle of time-scale separation holds. This means, that the change in state is much smaller than the change in control input ($\Delta x_c \ll \Delta u$) and we can, therefore, neglect the term depending on Δx_c. Furthermore, because f is not dependent on u, it also falls out of the term dependent on Δu. This greatly simplifies the incremental dynamics, which is now no longer dependent on function f, as shown in equation 20.

$$\dot{x}_c \simeq \dot{x}_{c,0} + G(x_0, p)\Delta u \tag{20}$$

Define v as the reference for $\dot{x}_c$, and $\hat{\dot{x}}_{c,0}$ and $\hat{p}$ as the state derivative and parameter vector estimates respectively. If G is invertible, equation 20 can be inverted to obtain the INDI control law as presented in equation 21. Here Δu_d is the desired control input increment, which is, for the rest of the derivation, assumed to be equal to the actual control input increment.

$$\Delta u_d = G(\hat{x}_0, \hat{p})^{-1}[v - \hat{\dot{x}}_{c,0}] \tag{21}$$

If one substitutes the control law (Eq. 21) into equation 20, the resulting dynamics of the controlled system appear as in equation 22. It can be seen that in the ideal case, when all estimates are perfect, the controlled system dynamics become linear. However, in reality, some non-linearities will always remain. One can, however, see that these non-linearities are much smaller than before. Firstly, the uncertainty in f no longer influences the non-linearities. Secondly, the term $[v - \hat{\dot{x}}_{c,0}]$, which is multiplied with the remaining non-linearity in G, is the error in angular acceleration. This term is generally much smaller than $[v - f(\hat{x}, \hat{p})]$, which is the multiplier for NDI. Therefore, the non-linearity in G has less effect for INDI than for NDI.

$$\dot{x}_c = \dot{x}_{c,0} + G(x_0, p)G(\hat{x}_0, \hat{p})^{-1}[v - \hat{\dot{x}}_{c,0}] \tag{22}$$

The total control input is obtained by adding the increment to an estimate of the current control surface deflection.

$$u = \hat{u}_0 + \Delta u \tag{23}$$

The fundamental advantage of INDI over NDI is that it is less model dependent and therefore more fault tolerant. INDI is, however, more dependent on sensor feedback, because estimates of the state derivatives and control surface deflections are needed. Finally, these estimates need to be synchronised, as the control increment is based on a linearisation around a specific point in time.

The controller based on INDI, which has been used in this research, is made and described by Grondman. [3] His controller uses INDI with a two degree of freedom outer loop design. In pitch and roll, the pilot has rate command attitude hold control at lower angles and has direct attitude control at higher angles. In yaw, the controller stabilises the sideslip angle around zero. Furthermore, the controller uses pseudo control hedging (PCH) to handle actuator saturation. The full structure of this controller will not be discussed any further in this paper, but can be found in [3].

C. Incremental Backstepping

The incremental backstepping (IBS) based control law consists of two parts, the inner loop which uses IBS to control the angular rates, and the outer loop which uses Backstipping (BKS) to generate a reference for the angular rates from the control variables $[\phi \ \alpha \ \beta]^T$. First BKS will be explained using the kinematics equations of the outer loop as example. Then IBS will be explained using the inner loop dynamics. Lastly the principle of command filtering and its effect on the control law will be explained.

8

Backstepping

BKS control is based on Lyapunov stability functions. A Lyapunov stability function is defined as any function V that is semi-positive definite and which time derivative $\dot{V}$ is semi-negative definite. If a fuction is a Lyapunov function it can be proven that the variables in this function are stable. This principle is used by making the Lyapunov function, depend on the tracking error, called a control lyapunov function (CLF). The simplest CLF, which has been used by e.g. van Ekeren [2], is the square of the tracking error, which results in a BKS control law with added proportional control. In this research a more extensive Lyapuov function has been chosen, which includes an integeral control term as well. This Lyaponov function is shown in equation 25. The derivation shown is based on Sonneveld [10]. The tracking error is defined as $z_{\bullet} = x_{\bullet} - x_{\bullet,\mathrm{ref}}$ and the to be controlled states are defined as in equation 24.

$$x_1 = \begin{bmatrix} \phi \\ \alpha \\ \beta \end{bmatrix} \quad \text{and} \quad x_2 = \begin{bmatrix} p \\ q \\ r \end{bmatrix} \tag{24}$$

$$V_1 = \frac{1}{2} z_1 z_1^T + \frac{K_{1I}}{2} \int z_1 dt \int z_1^T dt \tag{25}$$

Taking the time derivative of the CLF V_1 gives.

$$\dot{V}_1 = z_1^T \dot{z}_1 + z_1^T K_{1I} \int z_1 dt = z_1^T (\dot{z}_1 + K_{1I} \int z_1 dt) \tag{26}$$

Here the time derivative of the tracking error is $\dot{z}_1 = \dot{x}_1 - \dot{x}_{1,\mathrm{ref}}$, where $\dot{x}_1$ can be rewritten in a form that is affine in x_2 by combining equations 11 and 9 to form equation 27.

$$\dot{x}_1 = \underbrace{\begin{bmatrix} 0 \\ \frac{1}{V \cos \beta} [A_x \sin \alpha + A_z \cos \alpha] \\ \frac{1}{V} [A_x \cos \alpha \sin \beta + A_y \cos \beta - A_z \sin \alpha \sin \beta] \end{bmatrix}}_{f_1} + \underbrace{\begin{bmatrix} 1 & \sin \phi \tan \theta & \tan \theta \cos \phi \\ -\cos \alpha \tan \beta & 1 & -\sin \alpha \tan \beta \\ \sin \alpha & 0 & -\cos \alpha \end{bmatrix}}_{G_1} x_2 \tag{27}$$

The time derivative of the tracking error is then show in equation 28. Substituting $\dot{z}_1$ in equation 26 gives the CLF derivative of equation 29. Because one cannot directly impose a value for the state x_2, the state is written here as $z_2 + x_{2,\mathrm{ref}}$. Now one can make a controller for $x_{2,\mathrm{ref}}$.

$$\dot{z}_1 = f_1 + G_1 x_2 - \dot{x}_{1,\mathrm{ref}} = f_1 + G_1 (z_2 + x_{2,\mathrm{ref}}) - \dot{x}_{1,\mathrm{ref}} \tag{28}$$

$$\dot{V}_1 = z_1^T (f_1 + G_1 (z_2 + x_{2,\mathrm{ref}}) - \dot{x}_{1,\mathrm{ref}} + K_{1I} \int z_1 dt) \tag{29}$$

BKS control design allows for freedom in chosing the control law, as long as the CLF derivative of the whole controller is negative definite. The control law chosen for $x_{2,\mathrm{ref}}$ in this research is shown in equation 30. The Lyapunov function derivative left after substituting equation 30 is shown in equation 31. This function is not negative definite due to the term $z_1^T G_1 z_2$, which will be taken care of in the IBS innerloop.

$$x_{2,\mathrm{ref}} = G_1^{-1} \left[\dot{x}_{1,\mathrm{ref}} - f_1 - K_{1I} \int z_1 dt - K_{1P} z_1 \right] \tag{30}$$

$$\dot{V}_1 = z_1^T (G_1 z_2 - K_{1P} z_1) \tag{31}$$

Incremental Backstepping

For the design of the inner IBS control law a combined inner and outer loop Lyapunov function is defined as in equation 32, of which the time derivative is shown in equation 33. Here $\dot{z}_2 = \dot{x}_2 - \dot{x}_{2,\mathrm{ref}}$ is directly substituted.

$$V = V_1 + V_2 = V_1 + \frac{1}{2} z_2 z_2^T + \frac{K_{2I}}{2} \int z_2 dt \int z_2^T dt \tag{32}$$

9

$$\dot{V} = \dot{V}_1 + z_2^T(\dot{x}_2 - \dot{x}_{2,\text{ref}} + K_{2I}\int z_2 dt) \tag{33}$$

The dynamics equation defining $\dot{x}_2$ (shown in equation 2) is rewritten in an incremental form by taking the first order Taylor expansion. This was already done for INDI with a general dynamics equation in section IV.B, equation 19. Following the same procedure with the dynamics for x_2 gives the icremental dyanmics from equation 34.

$$\dot{x}_2 \approx \dot{x}_{2,0} + \left.\frac{\partial}{\partial u}[I(p)^{-1}M_A(x, u, p)]\right|_{\substack{x=x_0 \\ u=u_0}} (u - u_0) = \dot{x}_{2,0} + G_2(x_0, u_0, p)\Delta u \tag{34}$$

Just like in section IV.B, the assumption of time scale separation has been taken to be able to neglect the moments independent of control input. Furthermore, the linearisation introduces the need to have estimates of the synchronised angular acceleration $\dot{x}_{2,0}$ and control surface deflections u_0. Martix G_2 is the control effectiveness matrix and is defined in equation 35. The only model related terms in G_2 are the control effectivenesses and the wing geometry.

$$G_2 = I^{-1}\frac{1}{2}\rho V_{\text{TAS}}^2 S \begin{bmatrix} bC_{l_{\delta a}} & 0 & bC_{l_{\delta r}} \\ 0 & \bar{c}C_{m_{\delta e}} & 0 \\ bC_{n_{\delta a}} & 0 & bC_{n_{\delta r}} \end{bmatrix} \tag{35}$$

Substituting the incremental dynamics of equation 34 and the expression for $\dot{V}_1$ from equation 30 in equation 33 gives the Lyapunov derivative in terms of the incremental control input as shown in equation 36. A reference for Δu can now be designed as shown in equation 37. Note that the control input reference Δu_d is assumed to be equal to Δu

$$\dot{V} = z_1^T(G_1 z_2 - K_{1P}z_1) + z_2^T(\dot{x}_{2,0} + G_2(x_0, u_0, p)\Delta u - \dot{x}_{2,\text{ref}} + K_{2I}\int z_2 dt) \tag{36}$$

$$\Delta u_d = G_2(\hat{x}_0, \hat{u}_0, \hat{p})^{-1}(\dot{x}_{2,\text{ref}} - \hat{\dot{x}}_{2,0} - G_1^T z_1 - K_{2I}\int z_2 dt - K_{2P}z_2) \tag{37}$$

The control increment from equation 37 has to be added to the current control deflection estimate, using equation 23, as is done for INDI. If all assumptions hold and the estimates of states, state derivatives, input and parameters are correct, the resulting CLF of the whole controller is now negative semi-definite as shown in equation 38.

$$\dot{V} = -z_1^T K_{1P}z_1 - z_2^T K_{2P}z_2 \tag{38}$$

In the final control law, the time derivative of the angular rate reference $\dot{x}_{2,\text{ref}}$ appears. For the current application, this term cannot be derived analytically, and therefore has to be found numerically. This is commonly done by means of a command filter. Farrell et al. have proven that command filtering can be included in the IBS derivation without losing the stability proof. [17]

For the derivation of CFIBS, the compensated tracking error is defined as $\bar{z}_1 = z_1 - \xi_1$. Here ξ_1 is defined by a stable linear filter, which can be designed freely as long as the assumptions in [17] still hold. For this derivation the stable filter from equation 39 is taken. [17] $\xi_2 = 0$, as there is no filter after the inner loop.

$$\dot{\xi}_1 = -K_{1P}\xi_1 + G_1(x_{2,\text{ref}} - x_{2,\text{com}}) \tag{39}$$

Using the definitions above, the CLF of equation 40, and the control law described by equations 41 and 42, the negative definite CLF derivative of equation 43 can be formed. This proves the stability of the CFIBS controller. One can see that the only difference with respect to the original IBS controller (eqs. 30 and 37) is that the compensated tracking error is used in the correction term $G_1^T \bar{z}_1$ in equation 42.

$$V = \frac{1}{2}\bar{z}_1^T \bar{z}_1 + \frac{K_{1I}}{2}\int z_1 dt \int z_1^T dt + \frac{1}{2}\bar{z}_2^T \bar{z}_2 + \frac{K_{2I}}{2}\int z_2 dt \int z_2^T dt \tag{40}$$

$$x_{2,\text{ref}} = G_1^{-1}\left[\dot{x}_{1,\text{ref}} - f_1 - K_{1I}\int z_1 dt - K_{1P}z_1\right] \tag{41}$$

$$\Delta u_d = G_2(\hat{x}_0, \hat{u}_0, \hat{p})^{-1}(\dot{x}_{2,\text{ref}} - \hat{\dot{x}}_{2,0} - G_1^T \bar{z}_1 - K_{2I}\int z_2 dt - K_{2P}z_2) \tag{42}$$

$$\dot{V} = -\bar{z}_1^T K_{1P} \bar{z}_1 - \bar{z}_2^T K_{2P} \bar{z}_2 \tag{43}$$

Using the compensated tracking error in the correction term, as done in the CFIBS control law, has a negligible effect on the controller response and is only useful to prove stability. The controller used in this research, however, uses Pseudo Control Hedging (PCH) to handle actuator saturation. Using PCH invalidates the stability proof for CFIBS as given by Farrell [17] and a new stability proof, including the effects of PCH, is outside the scope of this research. Because the stability proof is not valid when using PCH, it was chosen not to use the compensated tracking error, but instead use the original IBS control law of equations 30 and 37, while still using command filtering.

V. Controller Design and Implementation

As explained in section II, four controllers are needed for this research. An INDI controller and an IBS controller, both working with and without angular accelerometer feedback. The subsystems of the INDI controller, as made by Grondman, can be found in his paper [3]. In this section the controller subsystems for the IBS controller are discussed. Note that some subsystems are used by both the IBS and INDI controllers. In figure 2 the controller and subsystems are visualised in a block diagram.

In this section, first, the supporting subsystems for the IBS based controller and the adaptations needed for the angular accelerometers will be discussed. Then, the gain tuning procedure is outlined and the resulting gains are presented. Lastly, the simulation setup is discussed and the fault tolerance of the controllers in simulation is analysed.

(a) Elements around the controller

(b) Elements inside the controller
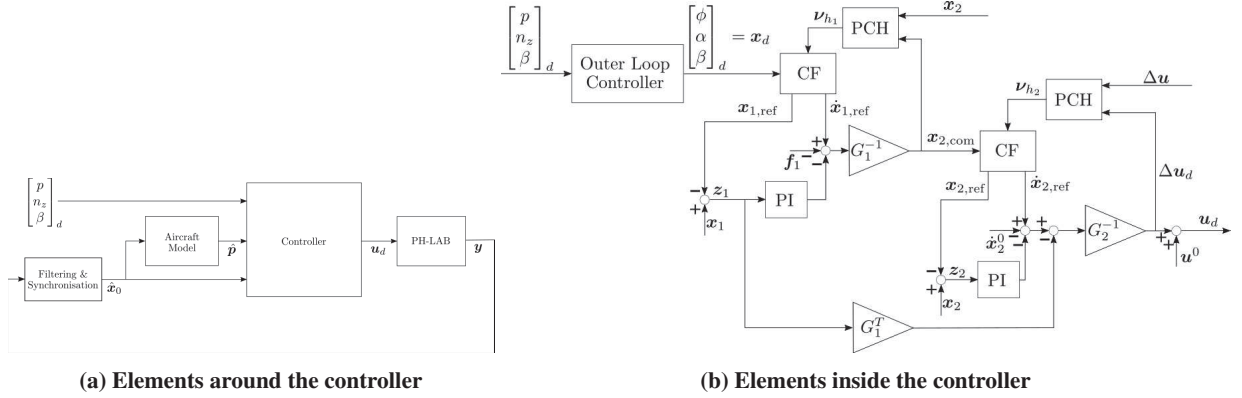
Fig. 2   Block diagram depicting the structure of the designed controller

A. Subsystems

Signal Filtering and Synchronisation
The signal filtering module of the controller processes all signals before they go into the controller. Because the incremental controllers are highly dependent on sensor feedback from the aircraft, it is important that this is done correctly. The signal filtering module is, except for the addition of the angular accelerometer filtering, the same as used by Grondman [3]. In this section, first, the special features from the signal filtering of Grondman will be summarised. Then the filtering and synchronisation of the actuator deflections, and angular rates and accelerations are discussed in more detail.

Grondman implemented complementary filters for airspeed, vertical speed, angle of attack, and sideslip angle to reduce the influence of atmospheric turbulence. The design of these complementary filters is based on Looye et al.[18]. The complementary filter used is shown in equation 44. Here subscript $_i$ indicates 'inertial'.

$$\hat{x} = \frac{1}{\tau s + 1} x + \frac{\tau s}{\tau s + 1} x_i \tag{44}$$

The inertial speed, vertical speed, angle of attack, and sideslip angle can be expressed as in equations 45, 46, 47, and 48 respectively. Note that the vertical speed $\hat{h}$ used in equation 47 is the complementary filtered vertical speed.

11

Furthermore, note that the time derivatives can directly be substituted for sx_i and no integration of equations 45, 46, and 48 is needed.

$$\dot{V}_i = \begin{bmatrix} A_x & A_y & A_z \end{bmatrix} \begin{bmatrix} \cos(\alpha)\cos(\beta) \\ \sin(\beta) \\ \sin(\alpha)\cos(\beta) \end{bmatrix} \qquad (45) \qquad \ddot{h}_i = \begin{bmatrix} A_x & A_y & A_z \end{bmatrix} \begin{bmatrix} \sin(\theta) \\ -\cos(\theta)\sin(\phi) \\ -\cos(\theta)\cos(\phi) \end{bmatrix} \qquad (46)$$

$$\alpha_i = \theta - \gamma_a, \quad \gamma_a \approx \frac{\hat{\dot{h}}}{V_{\text{TAS}}} \qquad (47) \qquad \dot{\beta}_i = \frac{f_y g + g\sin(\phi)\cos(\theta)}{V_{\text{TAS}}} - r\cos(\alpha) + p\sin(\alpha) \qquad (48)$$

When the angular accelerometer measurements are not used, the angular rate measurements are filtered by a second order low pass filter. The standard structure of such a filter is shown in equation 49, where for the angular rates $\omega_n = 20[rad/s]$ and $\zeta = 1$. The angular acceleration estimation is taken from this filter before the last integrator, and is, therefore, equal to $s\omega_{\text{fil}}$

When the angular accelerometer measurements are used, the filtered angular rates are obtained from a complementary filter. This complementary filter has the structure from equation 44, where the angular acceleration measurements are substituted for sx_i and the angular rate measurements for x. The filtered angular accelerations are obtained by filtering the angular accelerometer measurements with a second order filter with $\omega_n = 20[rad/s]$ and $\zeta = 1$.

$$H_{\text{fil}}(s) = \frac{\omega_n^2}{s^2 + 2\zeta\omega_n s + \omega_n^2} \qquad (49)$$

To ensure that the filtered control surface deflections are synchronised with the filtered angular accelerations, the filter and sensor delays of both signals need to be addressed. The filter delay is addressed by using the same filter for the control surface deflections as for the angular acceleration measurements. Thereafter, the difference in sensor delay is added to the signal with the least sensor delay. In this case, a 15 or 88 ms delay is added to the control surface deflection measurements, with or without angular accelerometers respectively. These numbers are based on the sensor models in section III.B.

Outer Loop Controller

The outer loop controller converts the pilot commands into commands for the IBS control variables $[\phi \ \alpha \ \beta]$. This conversion is implemented to improve the manual flyability of the controller. Below, the conversions made are explained for the roll and pitch axis. No conversion is made in the yaw axis.

In roll, the pilot has RCAH control at lower roll angles and direct attitude control at higher roll angles. The outer loop converts this to a pure roll angle control for the IBS controller by integrating the roll rate command in the RCAH domain and directly feeding through the roll angle command in the direct attitude control domain. Some logic has been implemented to make sure the switch between the two modes is smooth.

With the angle of attack as control variable it is hard to control the pitch axis manually, because the required angle of attack for steady flight changes with flight condition. A load factor outer loop has, therefore, been implemented to improve the manual flyability of the controller. The control law is shown in equation 50. Where $q = \frac{1}{2}\rho V^2$ is the dynamic pressure and S is the wing surface area.

$$\alpha_{\text{com}} = \frac{W}{C_{L_\alpha} q S} \int ((n_{z_{\text{com}}} - n_z)k_I + \dot{n}_{z_{\text{com}}})\text{dt} \qquad (50)$$

In this control law, the approximate relation between n_z and α is used to get a model based estimate of the required angle of attack command. To this, an integral controller is added to correct discrepancies in the model based estimate.

Pseudo Control Hedging

In this section Pseudo Control Hedging (PCH) is introduced as method to handle actuator saturation when the saturation deflection is unknown. In the derivations of the INDI and IBS controllers presented in section IV, the actuators are assumed to deflect instantaneously, while in reality they have their own dynamics. [9] In the current design, PCH hides the actuator dynamics from the control law, preventing the controller from reacting to these dynamics.

This is done taking the model based estimate of the angular acceleration as is done in equation 51. The angular acceleration deficiency introduced by the actuators is then calculated using equation 52. This value is then subtracted

from the angular rate command $x_{2,\text{com}}$ in the command filter. Note that the angular acceleration deficiency needs to be subtracted from the time derivative of $x_{2,\text{com}}$, but only influences $x_{2,\text{ref}}$ and not $\dot{x}_{2,\text{ref}}$.

$$\hat{\dot{x}}_2(\Delta u) = \dot{x}_{2,0} + G_2 \Delta u \tag{51}$$

$$\nu_{h_2} = \hat{\dot{x}}_2(\Delta u_d) - \hat{\dot{x}}_2(\Delta u) = G_2(\Delta u_d - \Delta u) \tag{52}$$

To avoid integrator wind-up in the BKS outer loop, PCH is implemented here as well. However, the outer loop PCH module is only activated at actuator saturation. The equation for the deficiency subtracted in the outer loop command filter is shown in equation 53. This term was calculated similarly to the inner loop deficiency.

$$\nu_{h_1} = G_1(x_{2,\text{com}} - x_2) \tag{53}$$

Controller Configurations
The controllers discussed in this paper are implemented on the aircraft as one big controller. This one controller is designed in such a way that the controller configuration can be changed easily during flight. The controller mode can be switched between open loop, NDI, INDI, or IBS control. For all controllers PCH and angular accelerometer feedback can be activated or deactivated. Note that for open loop control, PCH and angular accelerometer feedback have no influence.

B. Gain Tuning
The gains for the INDI based controller have been determined by Grondman [3] using the Multi Objective Parameter Synthesis Tool (MOPS) [8]. With this method the controller is optimised for a list of objectives, like rise time, overshoot, and sum of squared errors. This is combined with a multi-model approach in which MOPS is applied simultaneously for the nominal model and multiple models with model mismatch. The criteria and models used can be found in [3].

Due to time constraints, the gain tuning of the IBS based controller had to be done manually, based on engineering judgement. This resulted in the gains shown in table 2. It would have been preferable to tune the gains using an automatic tuning, such as the one used for the INDI controller. During tuning, however, care has been taken to avoid any sign of instabilities in the controlled variables.

Table 2   Gains used in the IBS based controller

	Proportional			Integral		
	Roll	Pitch	Yaw	Roll	Pitch	Yaw
IBS Inner Loop	5	3	1	3	6	1
IBS Outer Loop	1.5	1.5	0.5	0	1	0.2
n_z Outer Loop	-	-	-	-	0.5	-

C. Simulation of Fault Tolerance
In this section, fault tolerance of the controllers is discussed. The fault tolerance is determined by doing simulations in which the aircraft model is changed, but not the controllers' interpretation of the aircraft model. By doing this, model mismatch is introduced. An analysis has been done on the effect of mismatch in certain model parameters on the performance of the incremental controllers. The parameters that are changed can be the following:
- Control Effectivenesses
- Moments of Inertia
- Centre of gravity location
- Control surface deflections

The aircraft model and designed controllers are simulated in MATLAB/Simulink. The simulation runs real-time at a $1000Hz$ frequency using Heun's method for solving the differential equations. The low fidelity actuator model is used in the aircraft simulation. The high fidelity actuator model includes the experimental control input saturation, and, therefore, unnecessarily limits the controller fault tolerance. Furthermore, the controllers are all configured with PCH activated.

(a) without Angular Accelerometers

(b) with Angular Accelerometers
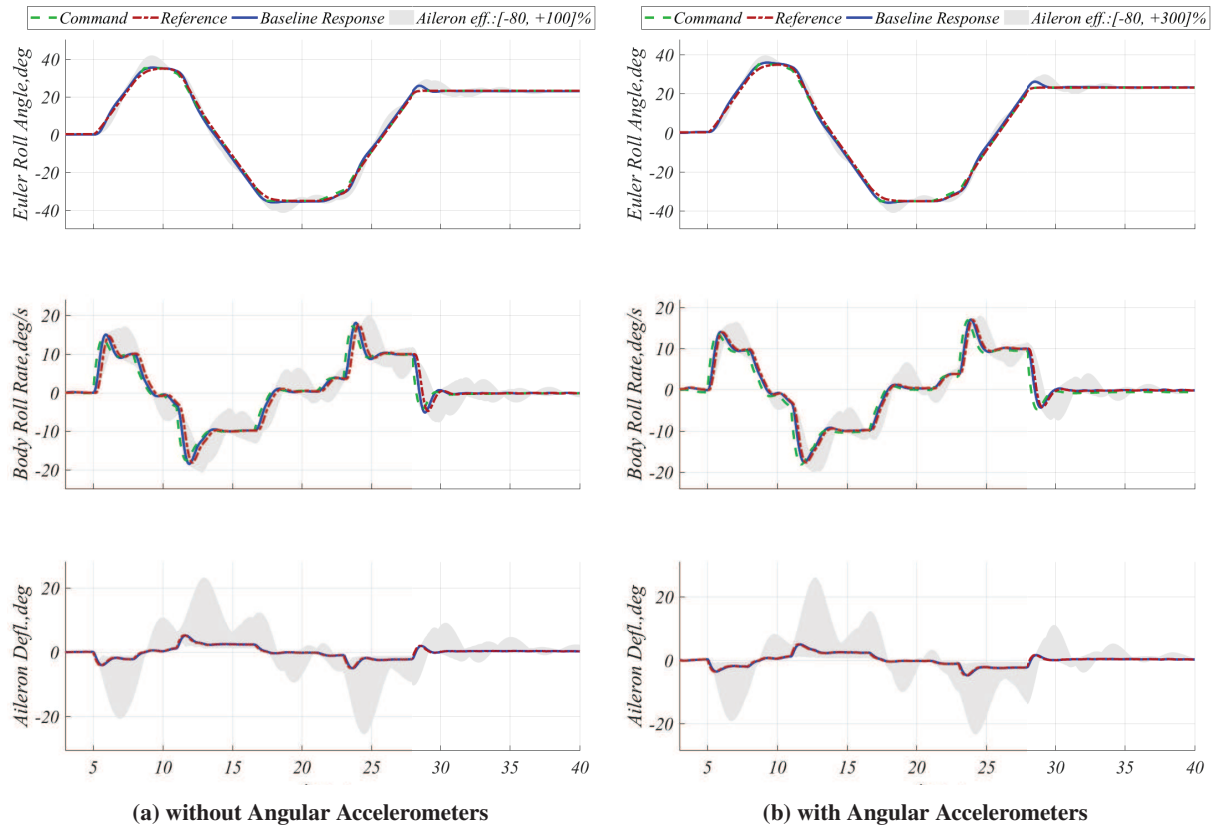
Fig. 3   Roll manoeuvre for IBS controllers with aileron effectiveness mismatch

Results are shown in figures 3 and 4 for the INDI and IBS controllers respectively, doing a roll manoeuvre with changed aileron effectiveness. In figures 5 and 6, results are shown for a pitch manoeuvre in which there is a mismatch in elevator deflection with respect to the trim. Changing the elevator deflection would require a re-trim for every simulated mismatch. This is not feasible with the current trim implementation.

Note that the reference signal is taken for the baseline case and that this reference changes for the different cases. The performance of the controllers is judged based on the error with respect to the nominal response and the occurrence of any oscillations or instabilities.

(a) without Angular Accelerometers　　　**(b) with Angular Accelerometers**
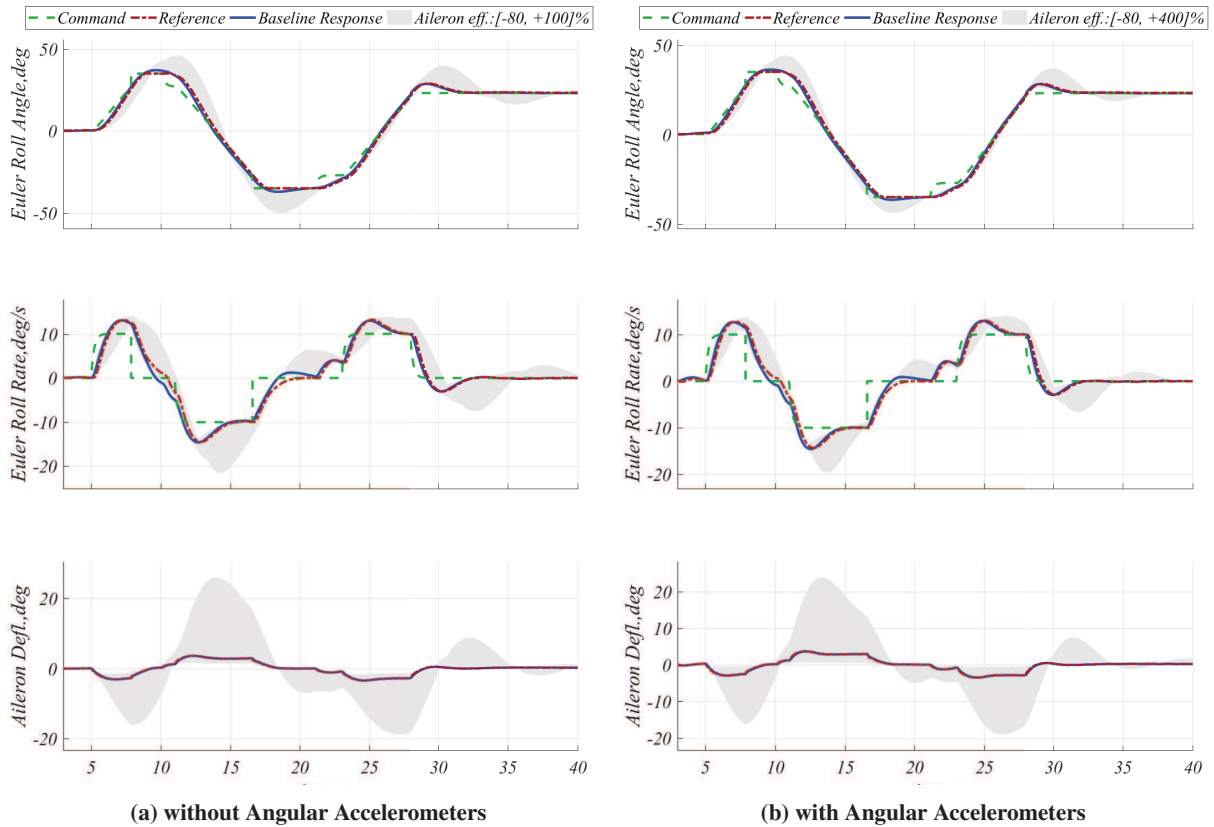
Fig. 4　Roll manoeuvre for INDI controllers with aileron effectiveness mismatch

As can be seen in figures 3 and 4, the range over which the aileron effectiveness can be changed is rather high, especially compared to the elevator.

The largest decrease in effectiveness shown is 80%, for all controllers. A larger decrease in effectiveness would result in actuator saturation, making the response significantly slower. However, for all controllers, the principle motion will still be followed even for larger decreases in effectiveness.

The largest increase in effectiveness shown is different per controller. For the IBS controllers, the largest increase in effectiveness is 100% without, and 300% with the angular accelerometers. A larger increase in effectiveness will for both controllers introduce a bounded amplitude oscillation with a maximum amplitude of $5deg$ in roll angle. This behaviour holds until at least a 1000% increase in effectiveness.

For the INDI controllers, the largest increase in effectiveness is 100% without, and 400% with the angular accelerometers. A slightly larger increase in effectiveness will for both controllers cause some small oscillations in the aileron and grow to a bounded amplitude oscillation with a maximum amplitude of $5deg$ in roll angle. This behaviour holds until at least a 1000% increase in effectiveness.

It can be concluded that using the angular accelerometer feedback in the incremental controllers increases their tolerance to aileron effectiveness mismatch. Furthermore it can be concluded that both incremental controllers are inherently tolerant to big changes in aileron effectiveness.

15

(a) without Angular Accelerometers

(b) with Angular Accelerometers
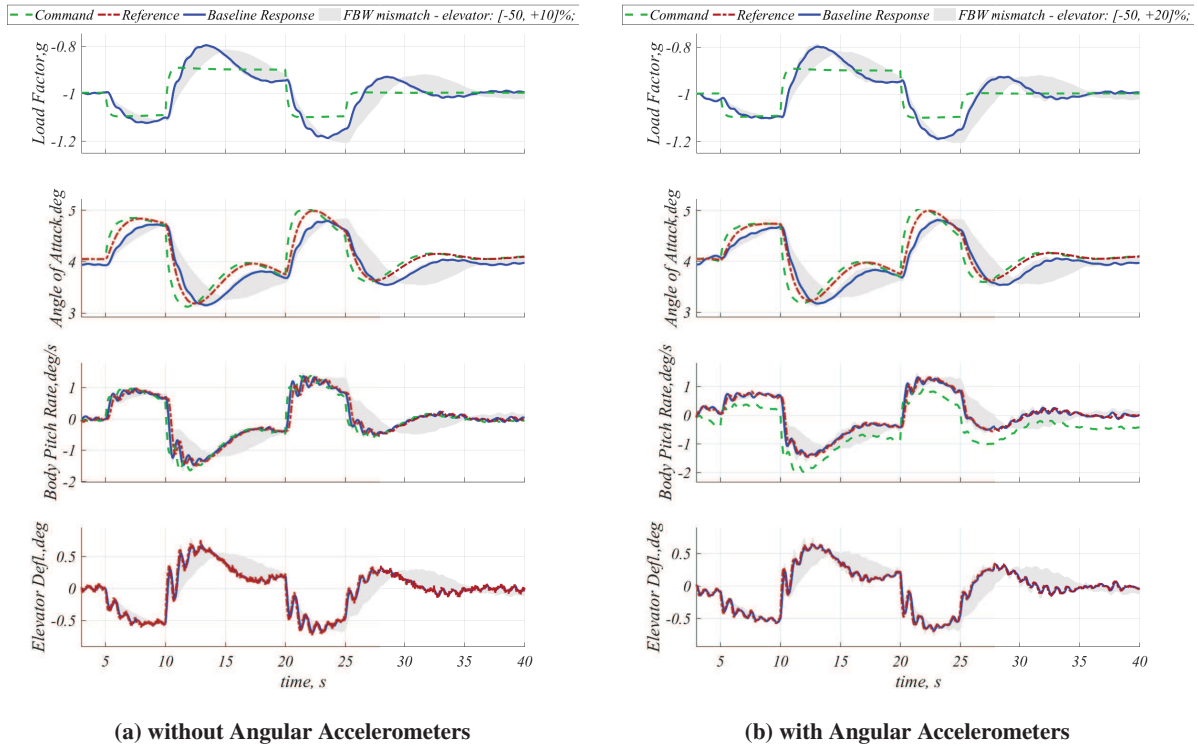
Fig. 5   Pitch manoeuvre for IBS controllers with elevator effectiveness mismatch

As can be seen in figures 5 and 6, the range over which the achieved elevator deflection can be changed is rather low, especially compared to the aileron.

The largest decrease in achieved deflection shown is 50%, for all controllers. A larger decrease in achieved deflection would make the response significantly slower, even though the saturation is not yet reached. However, for all controllers, the principle motion will still be followed even for larger decreases in achieved deflection.

The largest increase in achieved deflection shown is different per controller. For the IBS controllers, the largest increase in effectiveness is 10% without, and 20% with the angular accelerometers. A slightly larger increase in achieved deflection will for both controllers cause exaggerated oscillations in the elevator deflection, which will also become visible in the load factor. With an even larger increase in achieved deflection these oscillations will grow to a bounded amplitude oscillation with a maximum amplitude of $0.5g$ in load factor. This behaviour holds until at least a 500% increase in effectiveness.

For the INDI controllers, the largest increase in achieved deflection shown is 10% both without and with the angular accelerometers. A slightly larger increase in achieved deflection to 20% will for both controllers cause unstable oscillations.

It can be seen from figure 5 that the baseline response using the IBS controllers is already oscillatory in elevator deflection and pitch rate. Furthermore, it can be seen that these oscillations are barely visible in the angle of attack and load factor responses. Reducing the achieved elevator deflection makes the response smoother, but also slower. The current design was chosen as a compromise between speed and stability.

It can be concluded that using the angular accelerometer feedback in the IBS controllers increases their tolerance to achieved elevator deflection mismatch. For the INDI controller such a conclusion can not be made based on the available data. It is however expected that they follow the same trend, only on a smaller scale. Furthermore it can be concluded that both incremental controllers are inherently sensitive to achieved elevator deflection mismatch.
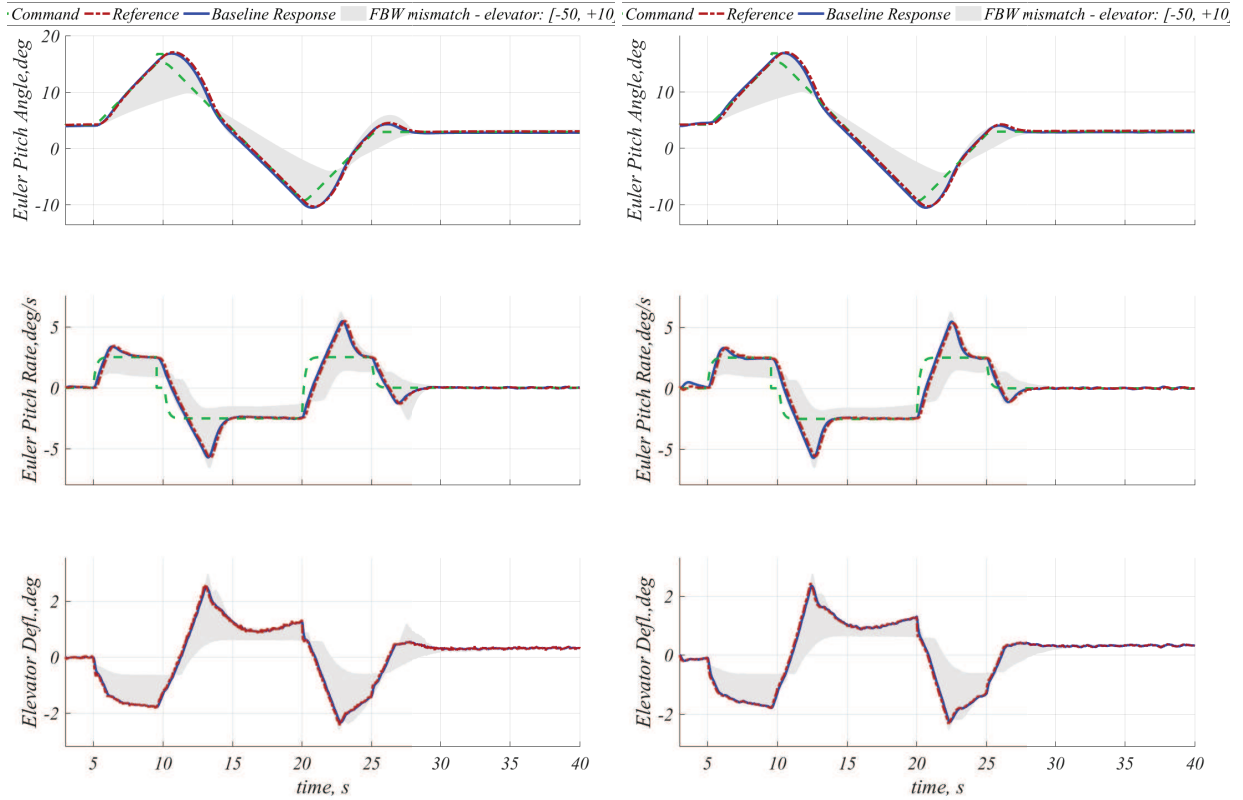
(a) without Angular Accelerometers

(b) with Angular Accelerometers

Fig. 6 Pitch manoeuvre for INDI controllers with elevator effectiveness mismatch

VI. Experimental Setup

The controllers designed in this research are made for implementation on the PH-LAB Cessna Citation II, as depicted in figure 1. This aircraft was originally an 8-passenger business jet, but it was modified to a research aircraft. With two Pratt and Whitney JT15D-4 engines providing a maximum of 11kN thrust each it has an operating ceiling at $43,000$ft at a maximum speed of 385kt.

A. Aircraft Configuration

The PH-LAB has a highly flexible configuration and is reconfigured to fit the needs of every flight test campaign. In this section the configuration during the flights done for this research will be discussed. First the Fly-By-Wire system and the software implementation of the controller will be discussed. Followed by the experimental sensors, and the pilot interfaces.

For this research a Fly-By-Wire (FBW) system was installed in the PH-LAB, allowing for the implementation of an experimental controller. The FBW system consists of among others of the following components: [19]

- Experimental Flight Computer, which runs the controller using the Delft University Environment for Communication and Activation (DUECA)
- Flight Test Instrumentation System (FTIS), which logs sensor measurements and control inputs, and communicates them with the Experimental Flight Computer.
- FBW Interface Box, which interfaces between the digital FTIS and the analog autopilot computer.

The experimental controller is compiled to C and implemented in the Delft University Environment for Communication and Activation (DUECA). DUECA assures real-time behaviour and handles all communication from the user and pilot input, to the controller output. A Graphical User Interface (GUI) is implemented in DUECA in which the flight test engineers can change the settings of the controller in-flight. For example, the controller configurations, controller

17

gains, and gains for the force stick can be changed. The GUI, in turn, interacts with the aircraft implementation of the controller. DUECA then sends the controller output to the FTIS. The controller output includes the logged signals for later analysis and the desired control surface deflections.

After the experimental controller, an internal proportional controller is used to track the desired control surface deflections. This controller could not be changed. The output of this controller is limited by a torque limiter on the electric servo actuators. Depending on the flight condition, this torque limit results in different deflection limits.

| (a) Sensor bay | (b) Pilot seat | (c) Pilot display |
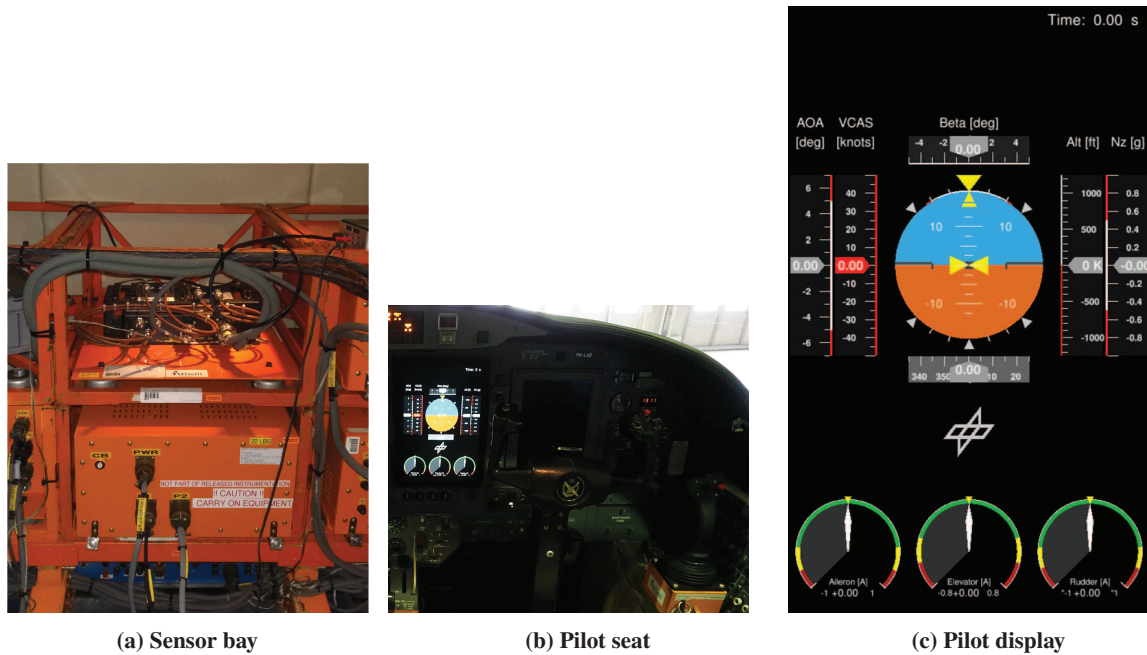
Fig. 7   Experimental Equipment in the PH-LAB

The experimental controller gets input from a force stick installed on the right hand side of the experimental pilot. (see figure 7b) Furthermore, an experimental pilot display was installed to the left of the experimental pilot. (see figure 7b) This display is designed to aid the pilots in flying the new controllers while at the same time showing basic information about the aircraft state. The display content is shown in figure 7c and displays the following information:

- Basic information on the aircraft state, such as velocity, altitude, attitude and heading.
- The current state and command for the control variables.
- Dials displaying the actuator currents, and showing the proximity to saturation.

Additionally, two experimental sensors are installed for the flight test. Firstly, the angular accelerometers are installed in the experimental sensor bay, which is located in the rear of the cabin. The angular accelerometers are installed in the middle box on the bottom of the experimental sensor bay as can be seen in figure 7a. Secondly, the air data boom was installed on the nose of the aircraft as can be seen in figure 1. The air data boom can measure angle of attack and sideslip angle in the undisturbed flow.

VII. Results

In this section the results from the flight tests are presented. First some nominal manoeuvres will be show, followed by results that demonstrate the fault tolerance of the controllers.

For all manoeuvres it can be seen that the control surface deflections do not always reach the reference set by the controller. This is due to the control of the actuator servos, which could not be altered. This means that unwillingly, tolerance to a certain level of control surface deflection mismatch has been proven in flight.

Furthermore, the hashed grey background shown in some plots indicates detected saturation of one of the control surfaces. The hash direction indicates which control surface is saturated. Elevator: \, Aileron: /, and Rudder: none. As discussed in section II, the outer loop PCH module is triggered on this saturation. Because the saturation characteristics of the actuators in-flight did not match the simulations, in some cases saturation was not correctly detected by the

18

controller. The saturations shown are the detected saturations. If these differ from the actual saturations, this is mentioned.

A. Nominal Manoeuvres

Roll Manoeuvres

(a) without angular accelerometer feedback

(b) with angular accelerometer feedback
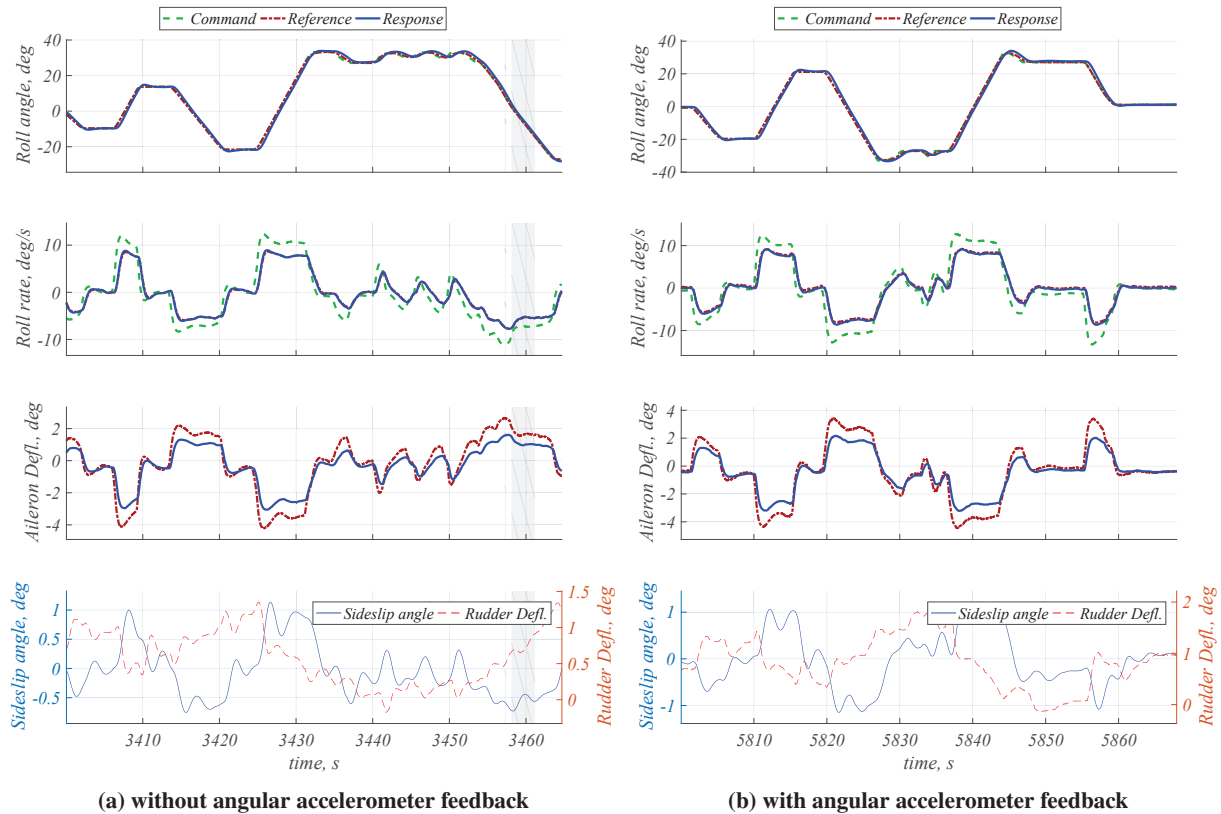
Fig. 8   Roll manoeuvre for IBS controllers

As can be seen in figure 8, the IBS controllers with and without angular accelerometer feedback show similar behaviour. Both IBS controllers track the roll angle command closely. For both, part of the roll rate command is removed by the inner loop PCH module. This causes the response to almost precisely overlay the reference. Furthermore, one can see that the reference aileron deflection, for both controllers, does not get reached completely by the actual control input. Lastly, one can see that for both controllers the sideslip angle is controlled to stay within approximately ± 1 *deg*.

For both controllers saturation occurs in the elevator. In figure 8b undetected saturation occurs shortly around 5830 seconds and for a longer period from 5845 to 5855 seconds. The elevator saturation, however, does not have an influence on the roll response.

As can be seen in figure 9, there is a noise in the roll rate response, aileron deflection reference and rudder deflection for the INDI controller without angular accelerometer feedback. This noise is not present in the response of the INDI controller with angular accelerometer feedback. This noise is not seen in any other manoeuvre with INDI or in the flight test results by Grondman. [3] It is, therefore, concluded not to attribute this behaviour to the INDI controller, but to disregard it as a singularity.

Disregarding the noise, the INDI controllers with and without angular accelerometer feedback show similar behaviour. Both INDI controllers track the roll angle and roll rate commands closely with a small delay. Furthermore, one can see that the reference aileron deflection, for both controllers, does not get reached completely by the actual control input.

(a) without angular accelerometer feedback

(b) with angular accelerometer feedback
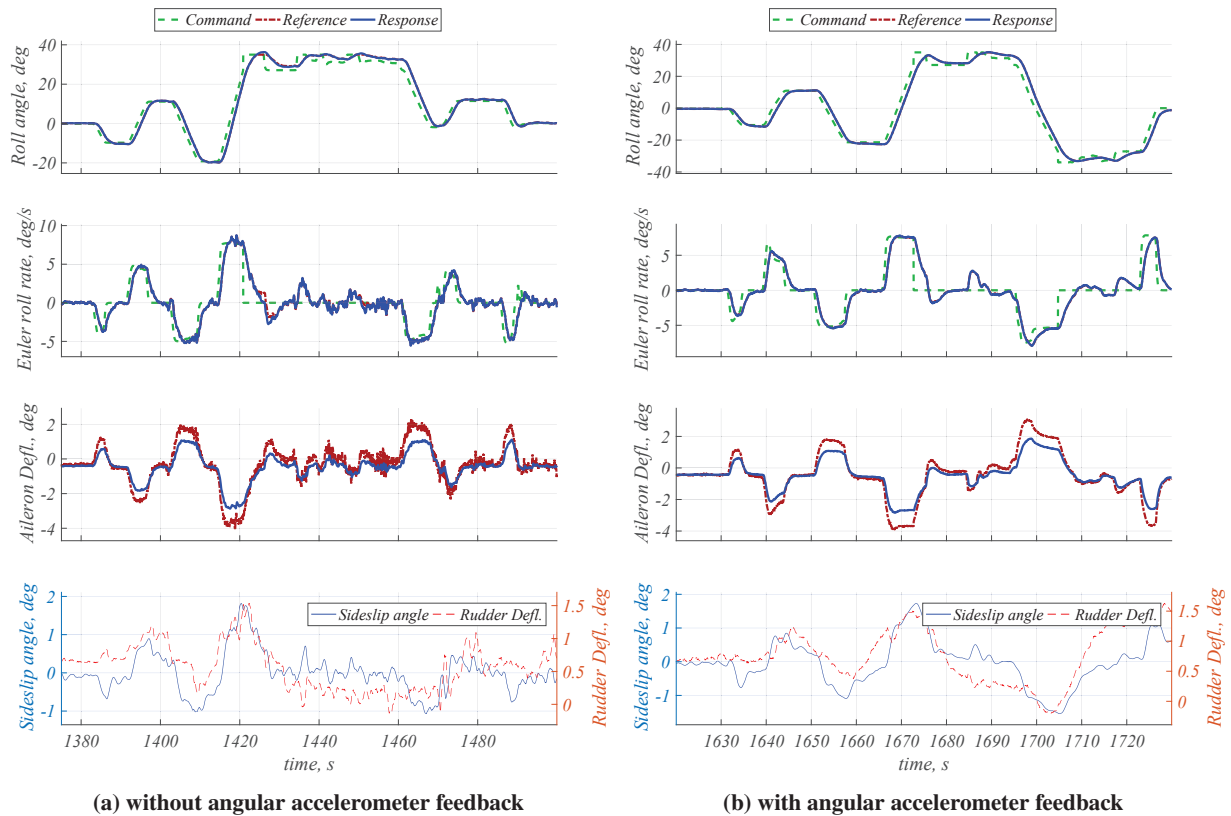
Fig. 9 Roll manoeuvre for INDI controllers

Lastly one can see that for both controllers the sideslip angle is controlled to stay within approximately ±2 *deg*.

Pitch Manoeuvres

As can be seen in figure 10, the tracking of the IBS controllers in load factor is less accurate than in roll angle. One can also see that the angle of attack tracking is again more accurate than the load factor tracking. Here, one should note that the load factor control is not part of the IBS control, but is controlled with a separate outer loop, which is only implemented to enhance manual flyability. The IBS controller performance should, therefore, be judged on the angle of attack tracking.

The angle of attack response follows the reference closely over most of the manoeuvres. At some points, however, for both controllers, the response can be seen to fall short. Furthermore, for both controllers, part of the pitch rate command is removed by the inner loop PCH module. One can see that, for the controller with angular accelerometers, the angular rate response does not overlay the reference. This is caused by a bias in the angular acceleration measurement. The angular rate depicted is the direct angular rate measurement. The angular rate estimate using the angular accelerometer measurements does exactly overlay the reference. Furthermore, one can see that the reference elevator deflection, for both controllers, does not get reached completely by the actual control input.

For the controller without angular acceleration feedback, in figure 10a, a very short saturation is detected in the elevator around 3347 seconds. Another short elevator saturation occurs around 3340 seconds, but is not detected. This saturation is short and happened while the tracking error was small. It, therefore does not have much impact on the response.

20

(a) without angular accelerometer feedback

(b) with angular accelerometer feedback
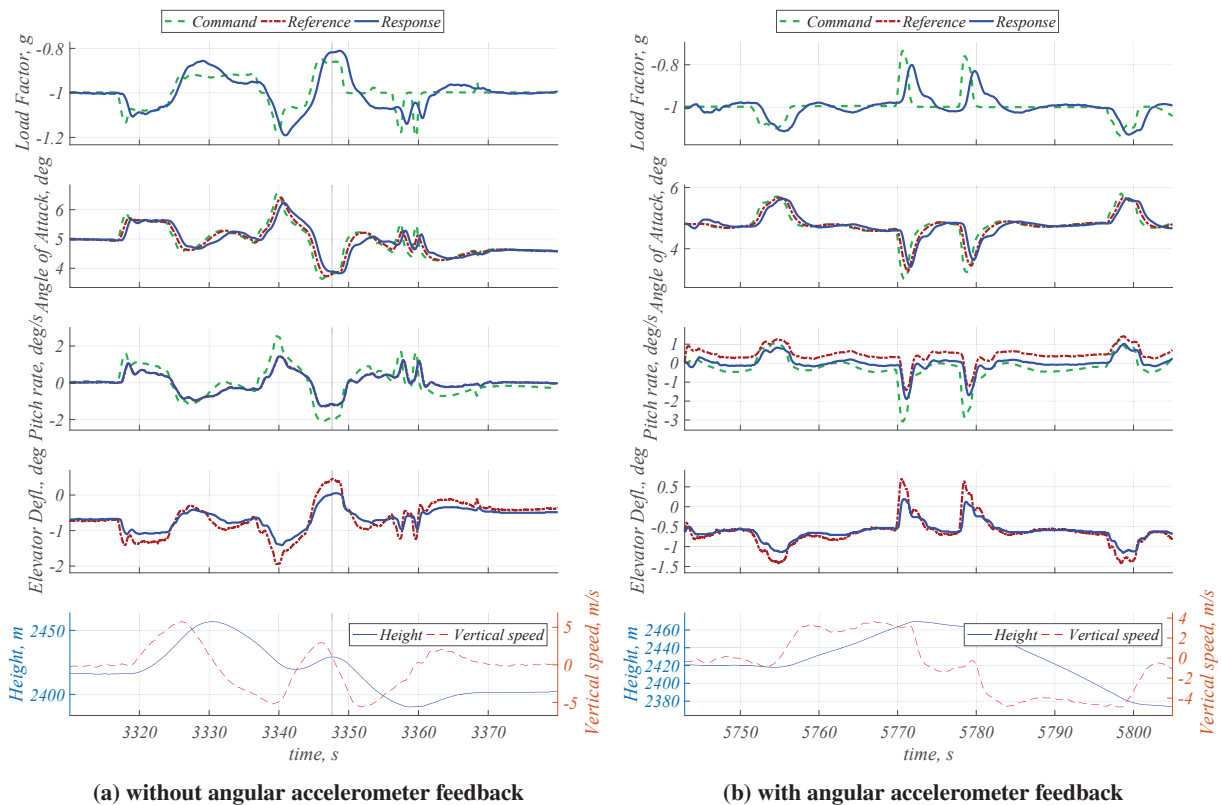
Fig. 10   Pitch manoeuvre for IBS controllers

Manoeuvres Demonstrating PCH

In this section two manoeuvres are shown in which the outer loop PCH module was working fully as intended. In figures 11 and 12 manoeuvres are shown in which saturations in the aileron and elevator are detected respectively.

For the manoeuvre shown in figure 11, a saturation in aileron deflection is detected. No separate outer loop is implemented here, and, therefore, the response should recover instantly after a saturation. This is also the behaviour that can be seen in figure 11b. The bump in roll rate command is caused by the initial error in roll angle between 7575 seconds and the saturation. This error is integrated by the integral control in the IBS inner loop.

For the manoeuvre shown in figure 12, a saturation in elevator deflection is detected. This, after a number of previous saturations were undetected. One can see that undetected saturations lead to overcompensation and largely delayed responses. The saturation is initiated by a manual re-trim just after 7720 seconds. This re-trim causes an uncommanded pitch up. Which the pilots react to with a pitch down command. This combination leads to saturation.

As soon as the saturation is detected, the outer loop PCH module adapts the angle of attack reference to follow the response. The series of undetected saturations around the one that is detected caused the pilots to give large control inputs. The elevator therefore gets into another saturation again almost directly after the detected one. One can however, see that the angle of attack reference is followed until approximately 7735 seconds. The PCH thus allows the reference to get followed again, however the situation in which it is activated causes another saturation almost directly after. If all saturations were detected the overall response would look much different.

(a) Pitch behaviour

(b) Roll behaviour
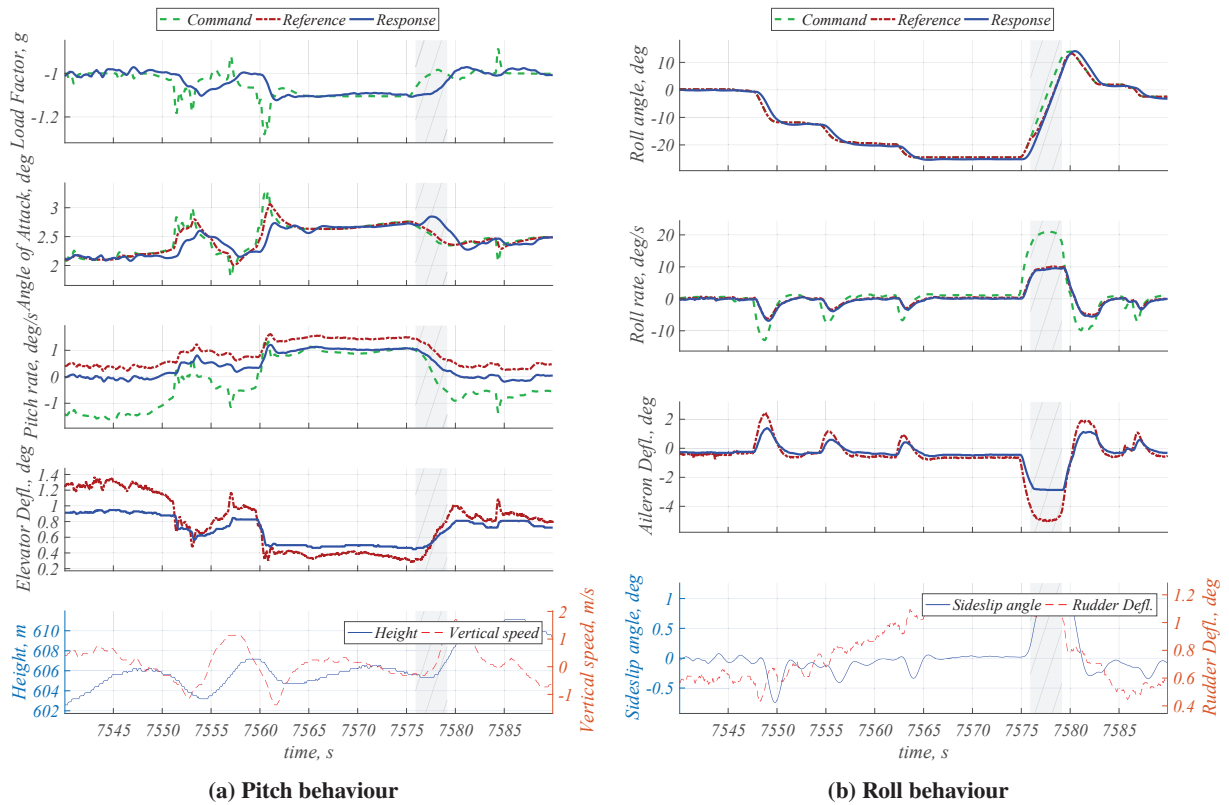
Fig. 11   Manoeuvre for IBS controller with angular accelerometers that demonstrates PCH

B. Off-nominal manoeuvres

In figure 13, One-Engine-Inoperative (OEI) manoeuvres with roll are shown for the IBS controllers with and without angular accelerometer feedback. One can see that for both controllers one engine is set to full power and the other to idle. Note that the side that is turned off is different for both controllers. For both controllers, the rudder is deflected automatically with the changes in fan speed. With this deflection, the sideslip angle is barely changed due to the asymmetric thrust. Furthermore, one can see that for both controllers the yaw rate is barely affected by the asymmetric thrust. Lastly, it can be seen that for both controllers a roll manoeuvre could be executed with performance similar to the nominal case.

Between the two controllers there is no difference in tracking performance. There are short areas of detected saturation in the rudder over the full manoeuvre. These areas are caused by a noisy rudder current signal, for which the noise peaks exceed the saturation current. These saturation areas are too short for the PCH module to have an effect.

C. Discussion

It should be stated that the INDI and IBS based controllers cannot be compared on their performance, neither in nominal performance, nor in fault tolerant behaviour. Both controllers are designed independently, with different control variables, outer loop designs and gain tuning methods. Both methods have been shown together only to demonstrate the wider applicability of the angular accelerometer feedback.

Furthermore it should be noted that the angular accelerometers used are not ideal for the current application. Of the $10[rad/s^2]$ range only 4% is used in the flight tests done. This caused relatively high noise levels and biases, most importantly introducing higher filter delay. Using better suited angular accelerometers is expected to improve the fault tolerance of the controllers even further.

Lastly, it should be noted that in the simulations done for fault tolerance, in the region near instability, the high fidelity actuator model did not always match the low fidelity actuator model used to generate the results presented in this paper. Note that this region of instability is far away from any of the responses shown in the figures.

(a) Pitch behaviour

(b) Roll behaviour
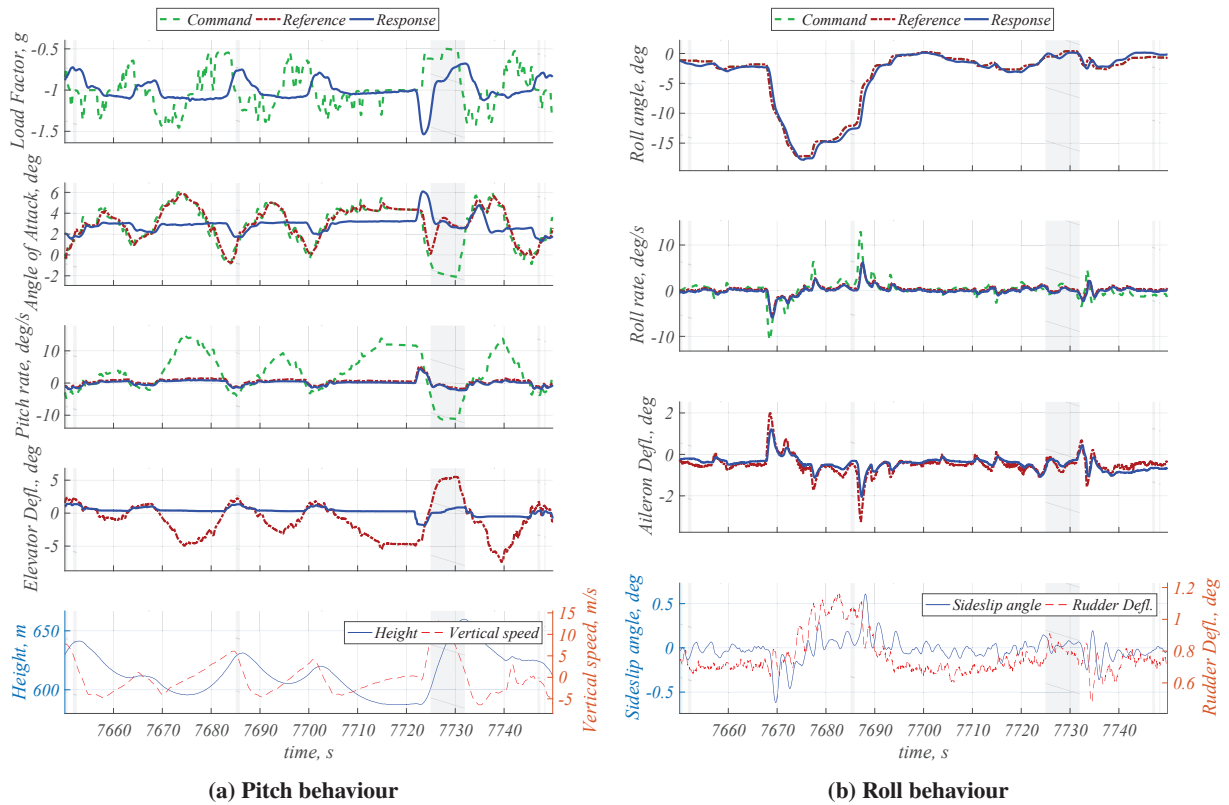
Fig. 12   Manoeuvre for IBS controller with angular accelerometers that demonstrates PCH

VIII. Conclusion

In this paper the design of an incremental backstepping (IBS) based control law with angular accelerometer feedback has been presented. This control law has been implemented in a non-linear simulation of the Cessna Citation II business jet and was subsequently flight tested on the PH-LAB research aircraft. In these flight tests the controller has proven to perform highly satisfactory.

The designed incremental backstepping controller uses an integrated integral control term in both loops for more tolerance to model mismatch. Furthermore, Pseudo Control Hedging (PCH) has been implemented to handle actuator saturation for unknown saturation deflections. Lastly, command filtering has been used to get the command derivatives between the backstepping loops.

This research marked the first flight with an IBS based control law on a CS-25 certified aircraft. The performance of the controller, both with and without angular accelerometer feedback was highly satisfactory. By using aerodynamic angles as control variables in pitch and yaw the potential of IBS as integrated multi-loop control law has been demonstrated as well.

Furthermore, this research marked the first successful integration of angular accelerometer feedback with incremental control laws. The angular accelerometers have been flight tested with both the newly designed IBS based controller and an Incremental Nonlinear Dynamic Inversion (INDI) based controller taken from preceding research. The angular accelerometer feedback has been found to have a negligible effect on performance in nominal flight.

In simulation, the fault tolerance of the incremental controllers with and without angular accelerometer feedback could be compared. In general the controllers using the angular accelerometer feedback proved to be more tolerant to model mismatches. A roll and pitch manoeuvre with aileron and elevator effectiveness mismatch, respectively, were simulated with and without the angular accelerometer feedback. In both cases the angular accelerometer feedback improved the tolerance to mismatch substantially.

In conclusion, angular accelerometer feedback does not improve the nominal performance of incremental controllers, but it does substantially increase the fault tolerance. Therefore the implementation of angular accelerometers on future

23

(a) without angular accelerometers

(b) with angular accelerometers
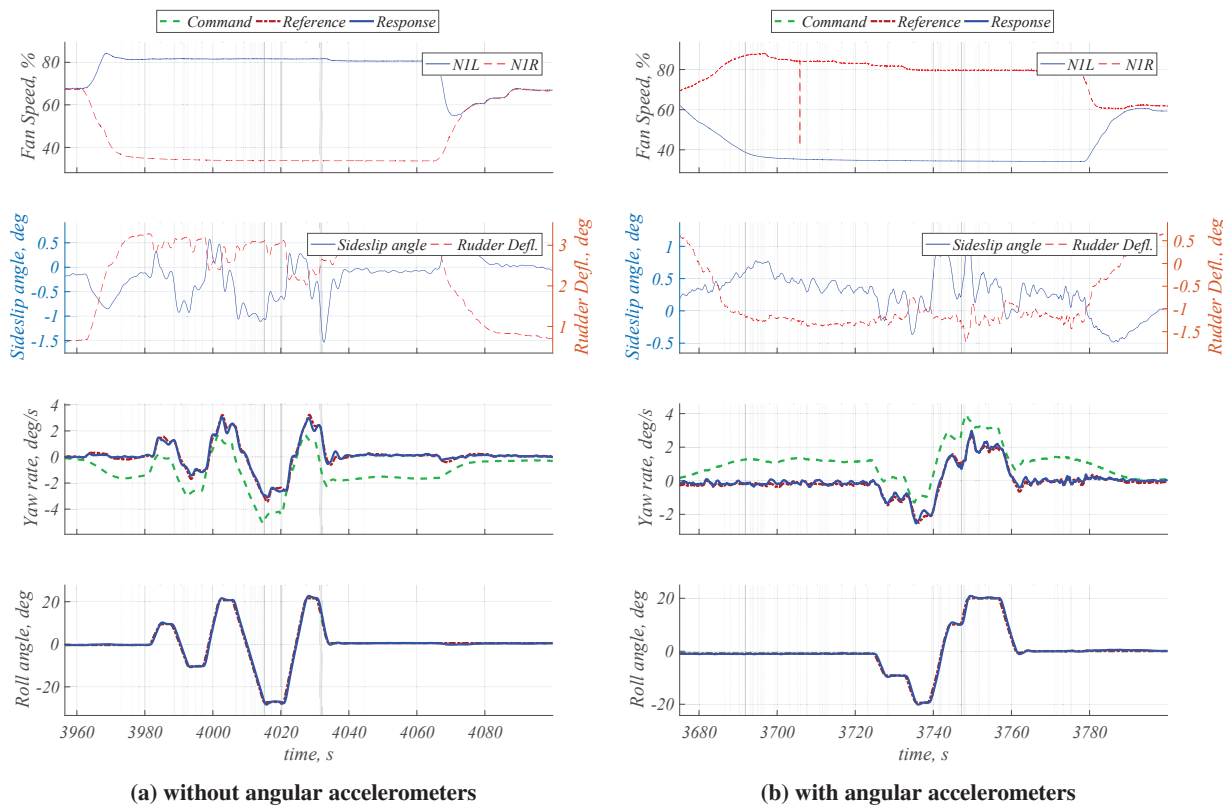
Fig. 13   OEI manoeuvre for IBS controllers

aircraft should be motivated by improving fault tolerance, rather than nominal performance.

References

[1] Vlaar, C., "Incremental Nonlinear Dynamic Inversion flight control - Implementation and flight test on a fixed wing UAV," Master's thesis, Delft University of Technology, Faculty of Aerospace Engineering, 2014.

[2] van Ekeren, W., Looye, G., Chu, Q., and van Kampen, E., "Design, Implementation and Flight-Tests of Incremental Nonlinear Flight Control Methods," *AIAA Guidance, Navigation, and Control Conference*, 2018.

[3] Grondman, F., Looye, G., Kuchar, R., Chu, Q., and van Kampen, E., "Design and Flight Testing of Incremental Nonlinear Dynamic Inversion based Control Laws for a Passenger Aircraft," *AIAA Guidance, Navigation, and Control Conference*, 2018.

[4] Smeur, E. J., Chu, Q., and de Croon, G. C., "Adaptive Incremental Nonlinear Dynamic Inversion for Attitude Control of Micro Aerial Vehicles," *Journal of Guidance Control and Dynamics*, Vol. 39, No. 3, 2016, pp. 450–461.

[5] Smith, P., and Berry, A., "Flight test experience of a non-linear dynamic inversion control law on the VAAC Harrier," *AIAA Atmospheric Flight Mechanics Conference*, 2000, pp. 132–142.

[6] Jatiningrum, D., de Visser, C., van Paassen, M., and Mulder, M., "Modeling an Angular Accelerometer using Frequency-Response Measurements," *AIAA Guidance, Navigation, and Control Conference*, 2016.

[7] Cakiroglu, C., Van Kampen, E.-J., and Chu, Q. P., "Robust Incremental Nonlinear Dynamic Inversion Control Using Angular Accelerometer Feedback," *AIAA Guidance, Navigation, and Control Conference*, 2018.

[8] Joos, H.-D., "A Methodology for Multi-Objective Design Assessment and Flight Control Syntheses Tuning," *Aerospace Science and Technology*, Vol. 3, No. 3, 1999, pp. 161 – 176.

[9] Johnson, E. N., and Calise, A. J., "Pseudo-Control Hedging : a New Method for Adaptive Control," *Advances in Navigation Guidance and Control Technology Workshop*, 2000.

[10] Sonneveld, L., "Adaptive Backstepping Flight Control for Modern Fighter Aircraft," Ph.D. thesis, Delft University of Technology, 7 2010.

[11] van der Linden, C., *DASMAT-Delft University Aircraft Simulation Model and Analysis Tool - A Matlab/Simulink Environment for Flight Dynamics and Control Analysis*, Delft University Press, Mekelweg 4, 2628CD Delft, The Netherlands, 1998.

[12] van den Hoek, M., de Visser, C., and Pool, D., "Identification of a Cessna Citation II Model Based on Flight Test Data," *4th CEAS Specialist Conference on Guidance, Navigation and Control: Warsaw, Poland*, 2017, pp. 259–277.

[13] van 't Veld, R., Van Kampen, E.-J., and Chu, Q. P., "Stability and Robustness Analysis and Improvements for Incremental Nonlinear Dynamic Inversion Control," *AIAA Guidance, Navigation, and Control Conference*, 2018.

[14] Mulder, M., Lubbers, B., Zaal, P., van Paassen, M., and Mulder, J., "Aerodynamic Hinge Moment Coefficient Estimation Using Automatic Fly-by-Wire Control Inputs," *AIAA Modeling and Simulation Technologies Conference and Exhibit*, 2009. doi:10.2514/6.2009-5692.

[15] Pollack, T., Looye, G. H., and van der Linden, F., "Design and flight testing of flight control laws integrating incremental nonlinear dynamic inversion and servo current control," , January 2019. Submitted to AIAA Guidance, Navigation, and Control Conference 2019.

[16] de Visser, C., "Global Nonlinear Model Identification with Multivariate Splines - Application to Aerodynamic Model Identification of the Cessna Citation II," Ph.D. thesis, Delft University of Technology, 5 2011.

[17] Farrell, J., Polycarpou, M., Sharma, M., and Dong, W., "Command Filtered Backstepping," *IEEE Transactions on Automatic Control*, Vol. 54, 2009, pp. 1391 – 1395.

[18] Looye, G. H., and Joos, H.-D., "Design of Robust Dynamic Inversion Control Laws using Multi-Objective Optimization," *AIAA Guidance, Navigation, and Control Conference*, 2001.

[19] Zaal, P., Pool, D., in 't Veld, A., Postema, F., Mulder, M., van Paassen, M., and Mulder, J., "Design and Certification of a Fly-by-Wire System with Minimal Impact on the Original Flight Controls," *AIAA Guidance, Navigation, and Control Conference*, 2009.